

Chapter 2

Diesel Engine Characteristics

Diesel engine is a compression ignition engine of a 2- or 4-stroke type. From the $p - V$ diagrams (Fig. 2.1), it can be seen that the duration of the whole diesel cycle is 360°CA for the *two-stroke engine* and 720°CA for the *four-stroke engine*. The whole cycle consists of the following *phases*: intake of air, compression of air, fuel injection, mixture formation, ignition, combustion, expansion, and exhaust. The intake phase begins with the intake valve opening and lasts till the intake valve closing. After that the intake air is compressed to a level corresponding to compression ratios from 14:1 to 25:1 (Bauer 1999) or even more. The compression ratio ε is a geometrical quantity, defined as

$$\varepsilon = \frac{V_{\max}}{V_{\min}} = \frac{V_h + V_c}{V_c}, \quad (2.1)$$

where V_{\max} and V_{\min} denote maximal and minimal volume above the piston, V_c is the clearance or compression volume, and V_h denotes the piston displacement—the volume between the bottom dead center (BDC) and the top dead center (TDC) of the piston.

Towards the end of compression, fuel is injected into the precombustion (indirect injection) or combustion (direct injection) chamber under high pressure. The fuel in the spray mixes with the compressed hot air, evaporates, and then the mixture ignites by itself. It has to be pointed out that injection, atomization, spray development, mixture formation, ignition, combustion, and emission formation processes proceed largely simultaneously and interact with each other. During the combustion process heat is released and both the in-cylinder pressure and the in-cylinder temperature increase. At the end of the expansion phase, the exhaust valve opens and the exhaust phase begins. This phase and the whole cycle end as the exhaust valve closes.

In automotive application, diesel engines are practically always of the 4-stroke type (Bauer 1999), either naturally aspirated or turbocharged.

In a *naturally aspirated diesel engine* (Fig. 2.2), the pressure p_k in the intake tubes is smaller than the ambient pressure p_o . Since at the end of the exhaust process the pressure p_r of the residual gases is higher than p_k , this means that the

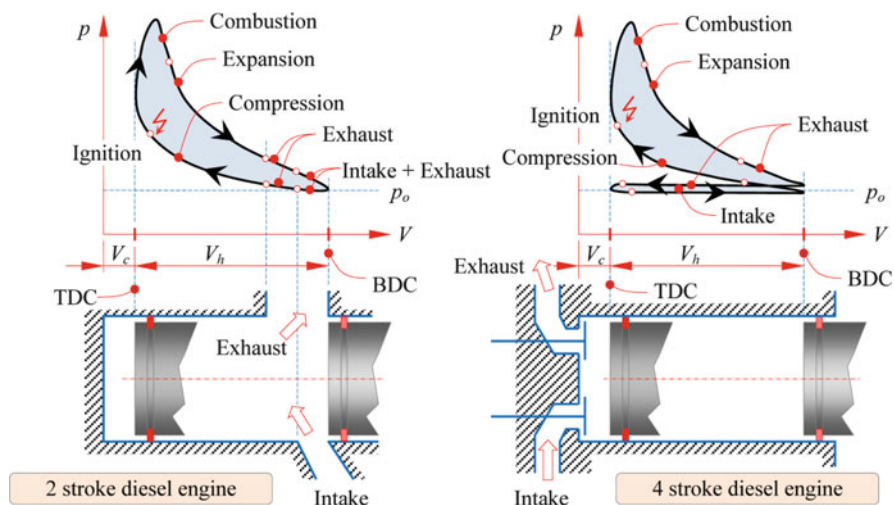


Fig. 2.1 The $p - V$ diagrams of two-stroke and four-stroke diesel engine

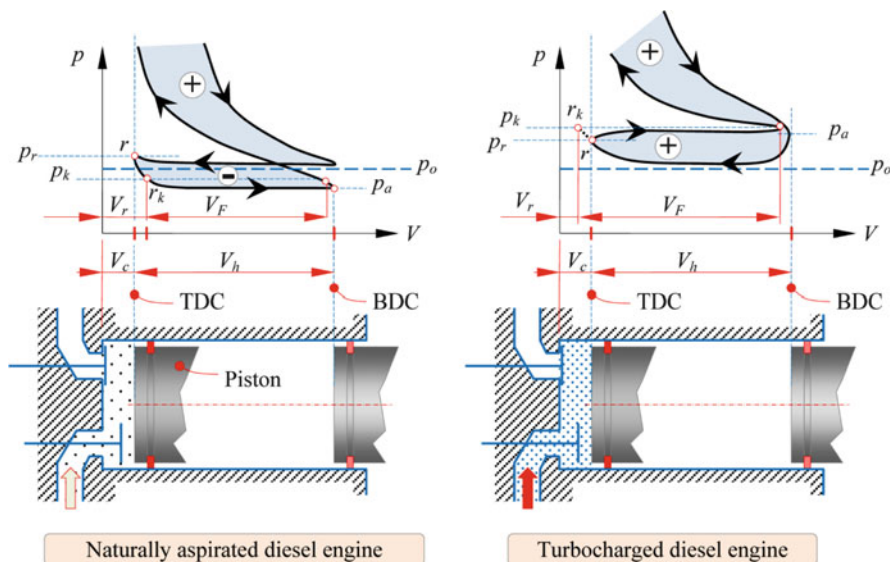


Fig. 2.2 The $p - V$ diagrams of naturally aspirated and turbocharged diesel engine

intake of air starts only after the piston travels a significant distance towards the bottom dead center. This means that the in-cylinder pressure p_a at the end of the intake process is always lower than p_k . In fact, in a naturally aspirated diesel engine the following relations are always valid: $p_r > p_k > p_a$ and $V_F < V_h$, where the symbol V_F denotes the actual volume of fresh intake air.

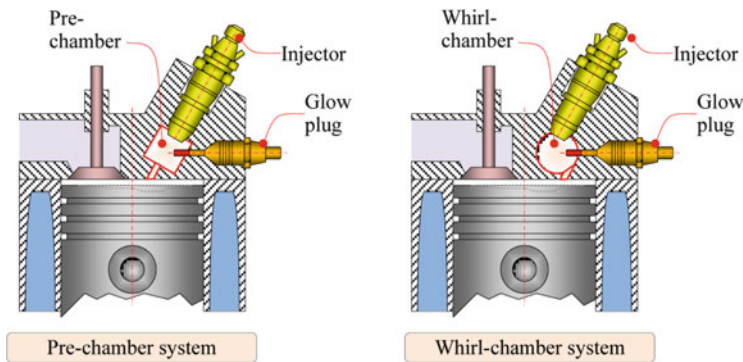


Fig. 2.3 Pre-chamber and whirl-chamber systems

In a *turbocharged diesel engine* (Fig. 2.2), the pressure in the intake tubes is higher than the pressure of the residual gases, i.e., $p_k > p_a > p_r$. This means that in spite of the residual gases and the hydraulic losses, the volume V_F of fresh air may be higher than V_h . In other words, the volumetric efficiency η_v , defined as

$$\eta_v = \frac{V_F}{V_h}, \quad (2.2)$$

can be higher than 1.0.

Fuel injection into the cylinder is realized by the fuel injection system, which can be of either an electronically (high pressure) or mechanically controlled type. More recent *electronically controlled injection systems* exhibit many advantages over the older mechanically controlled systems. In spite of that, one must admit that currently there are an enormous number of diesel engines with mechanically controlled systems still operating throughout the world. Moreover, *mechanically controlled injection systems* come with an attractive feature: they are very robust and relatively insensitive to fuel properties and quality. If the engine has to run on various biofuels, this can be a notable advantage.

Mechanically controlled fuel injection systems can be roughly classified as *direct* or *indirect injection systems*. Indirect systems inject the fuel into the pre-chamber or whirl chamber (Fig. 2.3), rather than directly into the cylinder. According to practical experiences in the past, one can roughly say that mechanically controlled indirect injection systems may deliver lower harmful emissions, especially of NO_x , compared to the direct injection systems. It is worth taking a brief look at this point.

At first, it has to be pointed out that in *indirect injection systems*, fuel is injected at a relatively low pressure up to 300 bar into the pre-chamber or whirl chamber when air is compressed through the piston movement to TDC. The injected fuel is mixed with the swirling air and the combustion starts in the pre-chamber (or whirl chamber), where the mixture is rich on fuel. Then, the air-fuel mixture is forced into the main combustion chamber and mixed with the residual compressed air. The combustion continues and completes in the main combustion chamber, where

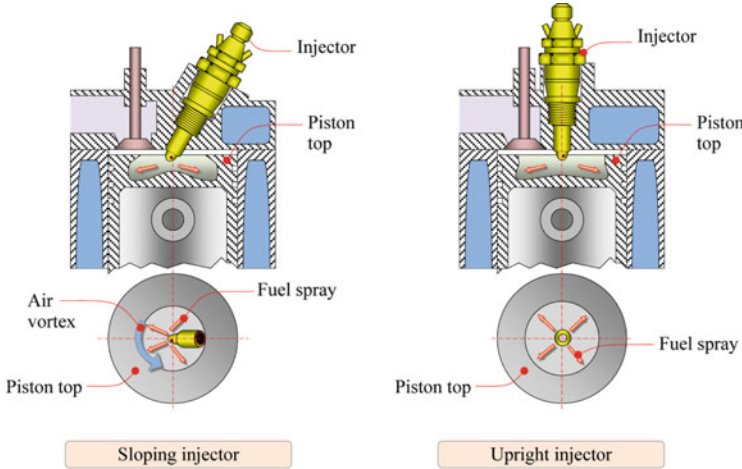


Fig. 2.4 Direct injection system—air distributed system

the mixture has a surplus of air. In this way, a two-phase combustion process is obtained: the first phase with a surplus of fuel, and at the second phase with a surplus of air. With an optimized pre-chamber or whirl chamber this can result in tempered release of energy at a low overall pressure level, soft combustion with low noise, low engine load, and low harmful emissions.

In *direct injection systems* fuel is injected with high injection pressure directly into the combustion chamber above the piston, using multi-hole nozzles. Here, fuel atomization, heating, evaporation, and mixture formation occur in very rapid succession. The air vortex is achieved by the special shape of the intake ports in the cylinder head. Furthermore, the design of the piston top with integrated combustion chamber contributes to the air movement at the end of the compression phase, when the injection process starts. Two fuel distribution methods are commonly used. The first one is the *air distributed method* (Fig. 2.4), where mixture formation is achieved by mixing fuel particles with air particles surrounding them.

The second method is the so-called *wall distribution method* (Fig. 2.5). In this, so-called *M fuel injection system* fuel is injected with a single-hole nozzle at relatively low pressure towards the walls of the combustion chamber. The fuel evaporates from the combustion chamber walls and is picked up by the swirling air. This method is characterized by extremely homogenous air–fuel mixtures, long combustion duration, low pressure rise, and soft combustion. However, the fuel consumption is higher compared to the air-distribution system.

The *features* of a diesel engine are defined by its *characteristics*. Diesel engine characteristics (Fig. 2.6) can roughly be classified into six groups as follows:

- *Fuel injection* characteristics
- *Fuel spray* characteristics
- *Combustion* characteristics

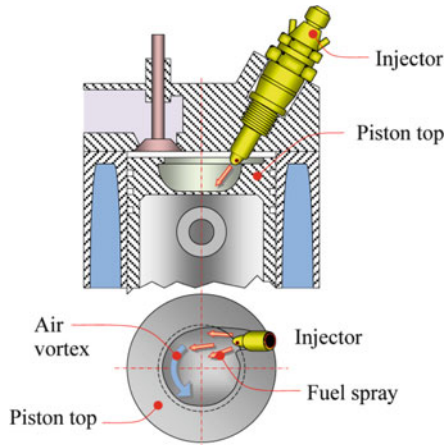


Fig. 2.5 Direct injection systems—wall distributed system

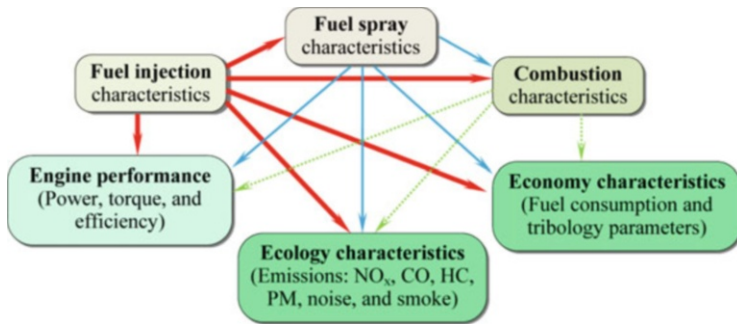


Fig. 2.6 Diesel engine characteristics

- *Engine performance* characteristics
- *Ecology* characteristics
- *Economy* characteristics

All these characteristics depend on the most basic parameters such as fuel type or injection system type and on various process characteristics such as the injection process, fuel spray development, atomization, mixture fuel/air formation, ignition and combustion, and so on (Merker et al. 2005). This means that even for a fixed engine type the diesel engine characteristics may be influenced by various geometrical and setup parameters. This holds true for a diesel engine with either mechanically or electronically controlled fuel injection system.

In *mechanically controlled injection systems*, like in-line, single, and distributor injection pumps, unit pumps, or unit injectors, the geometrical parameters play the most important role. Meanwhile, in *electronically controlled injection systems*, like common rail systems, engine behavior and performance are determined by setup parameters.

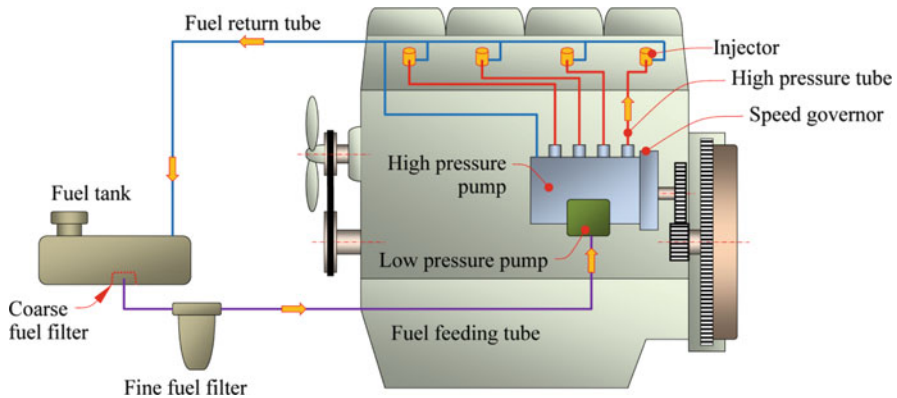


Fig. 2.7 Mechanically controlled in-line fuel injection system on a diesel engine

2.1 Injection Characteristics

The most important injection characteristics are (Kegl 1995, 1996):

- *Injection pressure*
- *Injection duration*
- *Injection timing*
- *Injection rate history*

All these characteristics influence the fuel spray formation, combustion process, engine performance, and consequently economy and ecology characteristics.

For a mechanically controlled fuel injection system, the injection characteristics depend strongly on its geometrical and setup parameters. Besides this, the injection characteristics can be influenced by the rest of the fuel path (Fig. 2.7), i.e., by the *coarse fuel filter*, *fine fuel filter*, *low pressure pump*, and so on.

The *mechanically controlled fuel injection system* consists basically of a high pressure fuel pump, high pressure tubes, and injectors (Kegl 1999). The *in-line fuel injection pump*, driven by a camshaft, has one pumping element for each cylinder. Pumping elements are mounted vertically in a straight line, side by side (Fig. 2.8). The lower half of the pump housing supports and encloses a horizontally positioned cam shaft, which has so many cam profiles as there are pumping elements. Each pumping element consists of a pump plunger which reciprocates in the barrel in dependence on camshaft profile. The camshaft profile converts the angular movement of the camshaft into a linear plunger motion by the roller cam follower and plunger return spring. Of course, the individual cam profiles are arranged according to the engine's firing order sequence. The top of each barrel is enclosed by its own delivery valve and optional snubber valve assembly.

The fuel enters the fuel ports at gallery pressure up to 1.5 bar, filling the space between the plunger and delivery valve. The plunger moves up in dependence on camshaft rotation following the cam profile and cuts off the feed/spill ports.

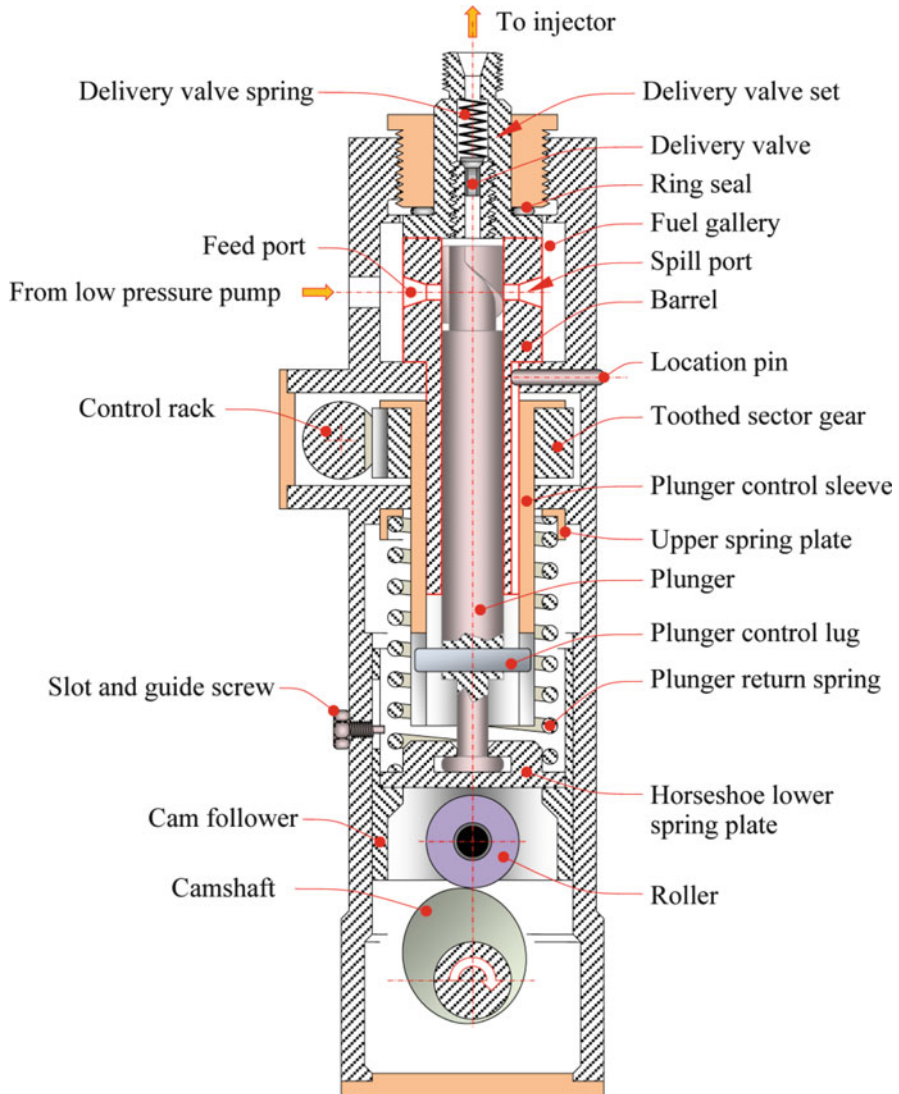


Fig. 2.8 Pumping elements

When all feed/spill ports are closed, the *geometrical fuel delivery begins* (Fig. 2.9). The in-barrel chamber pressure rises and eventually (dependent on the spring force and residual pressure in the high pressure tube) opens the delivery and the optional snubber valve. The pressure in the in-barrel chamber increases until the edge of the plunger helix unveils the feed/spill ports. Instantly, the in-barrel pressure collapses as fuel begins to escape down the vertical slot and exits through the feed/spill port. This is the moment of the *geometrical end of fuel delivery* (Fig. 2.9).

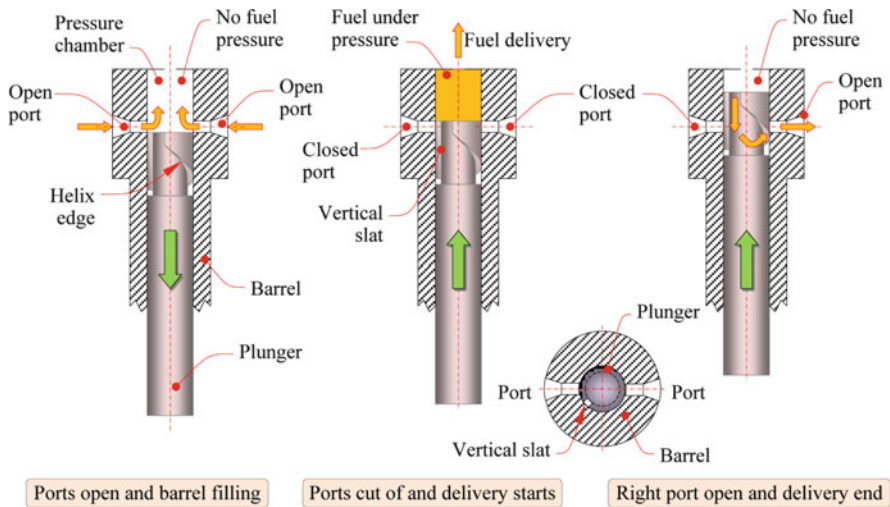


Fig. 2.9 Fuel delivery process with geometrical start and end of delivery

The pressure rise in the in-barrel results in a pressure wave traveling towards the injector. When this pressure wave reaches the injector nozzle (Fig. 2.10), the needle opens and the injection starts. After the fuel delivery ends, the pressure in the injector chamber falls, the needle closes, and the injection process terminates.

Injection pressure is the fuel pressure just before the injector nozzle holes. It depends on the type of injection system, on engine speed and load, and on fuel properties. Diesel engines with divided combustion chambers operate with high air speed in the pre-chamber or whirl chamber and main combustion chamber. Therefore, for indirect diesel engines, the injection pressure is typically about 350 bar. For direct injection diesel engines, however, air speed in the combustion chamber is relatively low. Therefore, in order to achieve satisfactory air/fuel mixing, the fuel has to be injected into the combustion chamber at high pressure, typically up to 1,000 bar. In order to get good overall engine performance, the injection pressure history should in general exhibit a high mean/peak pressure ration, i.e., no extreme pressure peaks. Figure 2.11 shows a typical injection pressure history and other injection characteristics.

Injection timing is the time span between the start of injection and the TDC of the engine piston. Injection timing has a strong influence on injection pressure, combustion process, and practically all engine emissions.

Injection duration is the time span from the beginning to the end of injection. In general, injection duration should be as short as possible. At higher engine speeds, injection duration should become longer and the mean injection pressure should be reduced (Desantes et al. 2004).

Injection rate represents the quantity of fuel injected per unit of time into the combustion chamber. Variations of injection rate history influence mixture preparation, combustion process, and harmful emissions. In a mechanical injection

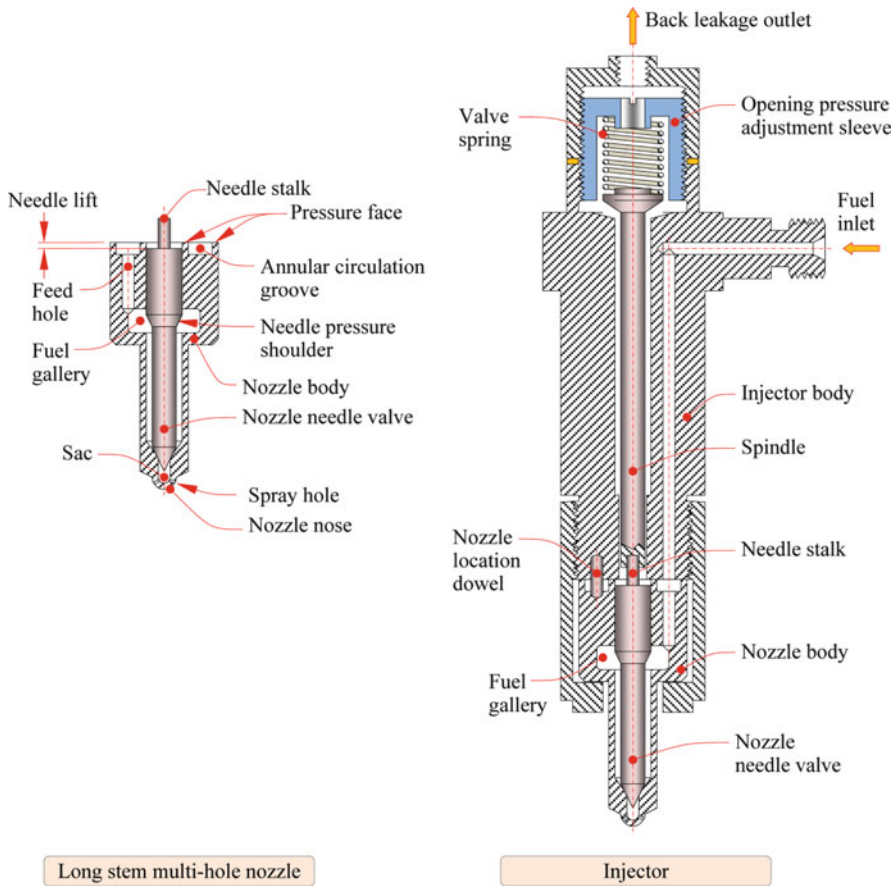


Fig. 2.10 Injector nozzle

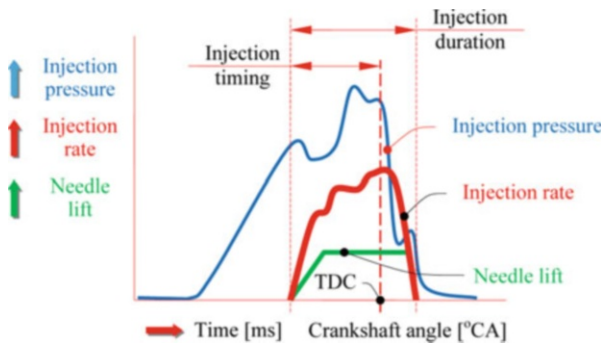


Fig. 2.11 Injection characteristics

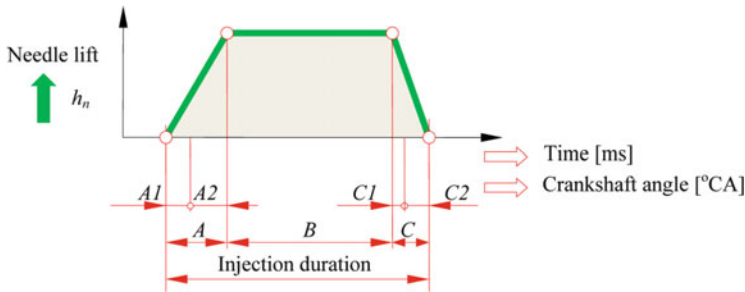


Fig. 2.12 Injection process phases

system the injection rate history is defined by the injection system design and varies in dependence on engine speed and load. Ideally, the injection system should deliver an optimal shape of the injection rate history in dependence on engine type and engine operating mode. Irrespective of this, it is possible to give some general guidelines as follows. Firstly, within the ignition delay, the injected fuel quantity has to be small while the main injection requires a steeply increased rate. Furthermore, with increasing engine speed and load, the fullness of the main injection should be raised, i.e., its shape should change from triangular to rectangular. To satisfy the above requirements, boot injection or split injection is an attractive option (Herzog 1989; Needham 1990).

For practical reasons it is convenient to distinguish between the following *phases of injection* (Fig. 2.12):

- Needle opening phase (A), which is subdivided into A1 (first 10 % of injection) and A2 (from end of A1 till the end of A)
- Open needle phase (B)
- Needle closing phase (C), which is subdivided into C1 (from start of C till the beginning of C2) and C2 (last 10 % of injection)

Throughout this book, the injection quantities (such as fuelling), corresponding to phase A, will be termed as partial quantity A, and so on for all other phases.

Figure 2.13 shows an example of quasi-ideal injection rate histories in dependence on engine operating conditions (Hwang et al. 1999).

Injection rate history is a very important characteristic. It strongly depends on the *delivery rate history* and it has the most important influence on the *heat release rate* (Fig. 2.14). The *delivery rate* is the quantity of fuel pushed per unit of time through the delivery valve into the high pressure tube. It is mainly influenced by the pump plunger diameter and pump plunger velocity, which depend on the cam profile. For example, a concave cam profile results in pump plunger velocity being higher than that obtained by the tangential or convex profile (Ishiwata et al. 1994; Kegl and Müller 1997; Kegl 1999, 2004). The actual start of fuel delivery depends on *injection pump timing*, which is usually given in crankshaft angle before TDC and indicates the moment when the pump plunger begins compressing the fuel. The delivery rate history is a well-controllable characteristic. The time from delivery

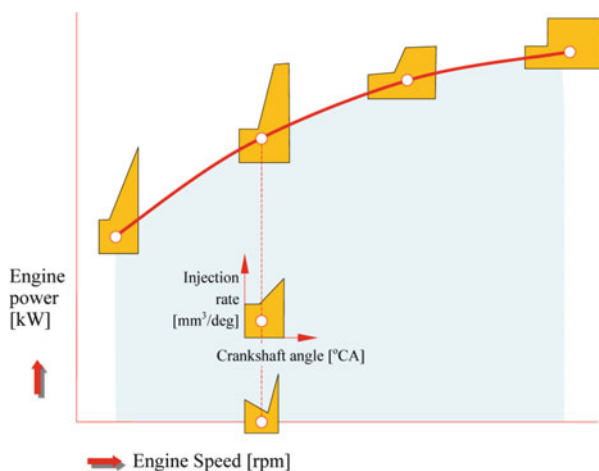


Fig. 2.13 Ideal injection rate shapes at various engine regimes

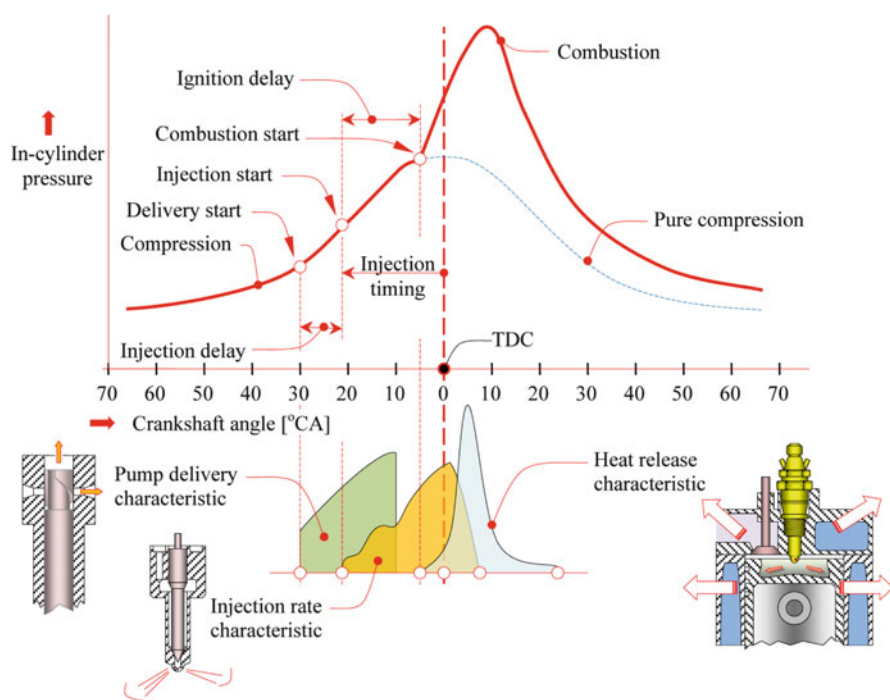


Fig. 2.14 Delivery rate history, injection rate history, heat release, and in-cylinder pressure

start to the *injection start* is the *injection delay*. The moment of injection start, given in crankshaft angle before TDC, is called the *injection timing*. Injection timing depends to a great extent on fuel properties and on geometrical parameters of the pump, high pressure tube, and injector. All these parameters influence the *injection*

rate history. For this reason, injection rate history, injection start, and injection end are rather difficult controllable quantities. After injection start the fuel atomizes, evaporates, and mixes with air until the mixture ignites. The time span between the injection start and combustion start is termed the *ignition delay*. The ignition delay, injection rate, and combustion chamber design influence strongly the *heat release rate history*. Therefore, heat release rate is also a rather difficult controllable quantity.

It is obvious that the dependencies between various injection characteristics and other involved quantities are rather sophisticated. Therefore, it makes a good sense to investigate these relationships as much as possible. For this purpose experimental techniques and mathematical modeling with numerical simulation have to be employed.

2.1.1 Experimental Techniques

For a mechanically controlled fuel injection system the most basic test bench should allow to measure the pressures immediately after the pump and before the injector as well as the needle lift and fuelling. Figure 2.15 illustrates possible positions of pressure and needle lift transducers (Kegl 2006; Kegl and Hribernik 2006).

The whole test bed of a fuel injection system should look something like the one depicted schematically in Fig. 2.16. One pressure transducer (e.g., a diaphragm type transducer) is located at the high pressure tube inflow just behind the injection pump. Another pressure transducer (e.g., a piezoelectric pressure transducer) is located at the high pressure tube just before the injector. The needle lift and the TDC position can be measured by a specially designed variable-inductance sensor and by an optic sensor, respectively.

The injected fuel quantity is typically measured by collecting the injected fuel over 500 cycles into a test glass. The fuel temperature is measured at the inflow into and after the pump in order to account for possible fuel quantity correction. The testing has to be performed at various temperatures. However, *low temperature testing* requires the most attention. For example, a special cooling system has to be developed and attached to the test bed in order to maintain the desired preset constant temperature conditions. A possible setup with two separated cooling systems, conditioning the fuel injection pump and fuel, respectively, is presented in Fig. 2.17 (Kegl and Hribernik 2006; Kegl 2006). In this setup the fuel injection pump is placed into an isolated metal case and connected to the electric motor drive of the test bench by a rigid shaft. Plate evaporators can be used as inner case walls in order to dispose sufficient energy to maintain temperatures well below the ambient one. A PID controller can be applied for temperature control in order to ensure the tolerances of the set temperature to be within ± 0.5 °C. Injectors should be mounted outside of the cooled case in order to enable simple measurement of the injected fuel amount. They can be connected to the injection pump by standard thermally isolated high pressure tubes. The fuel supply forms the second cooling system. A large fuel tank (e.g., 50 L) is placed into a refrigerator,

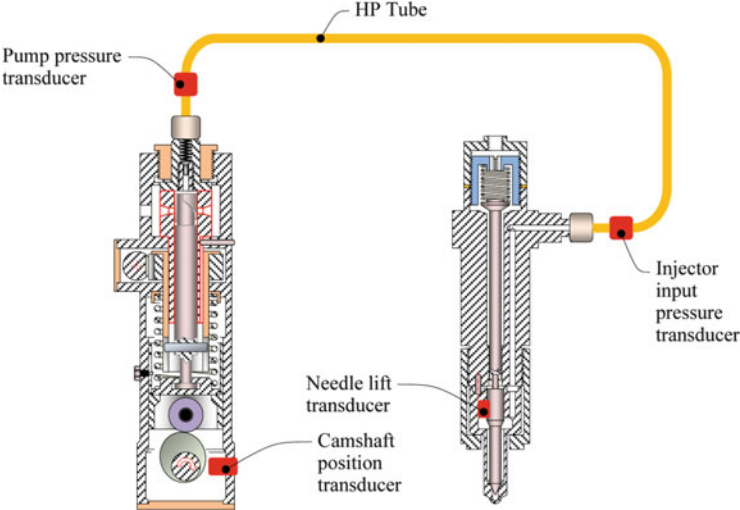


Fig. 2.15 Positions of transducers

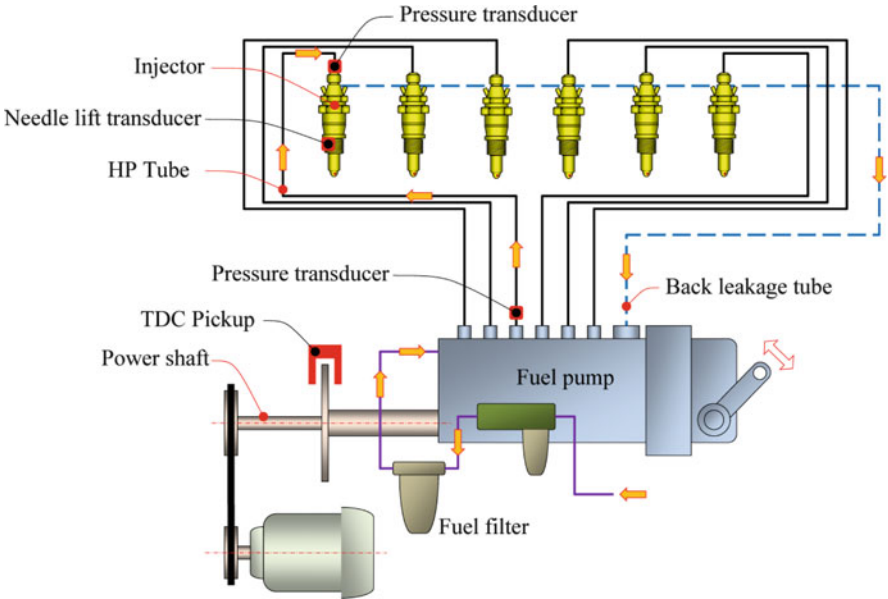


Fig. 2.16 Fuel injection system test bed

which allows the temperature to be controlled in the range between $-30\text{ }^{\circ}\text{C}$ and $40\text{ }^{\circ}\text{C}$. An ice-cooled heat exchanger, i.e., a pipe coil frozen within the ice cube, is placed next to the fuel tank. This exchanger cools the fuel flowing from the injection pump back to the fuel tank. This back flow can then be mixed with cool

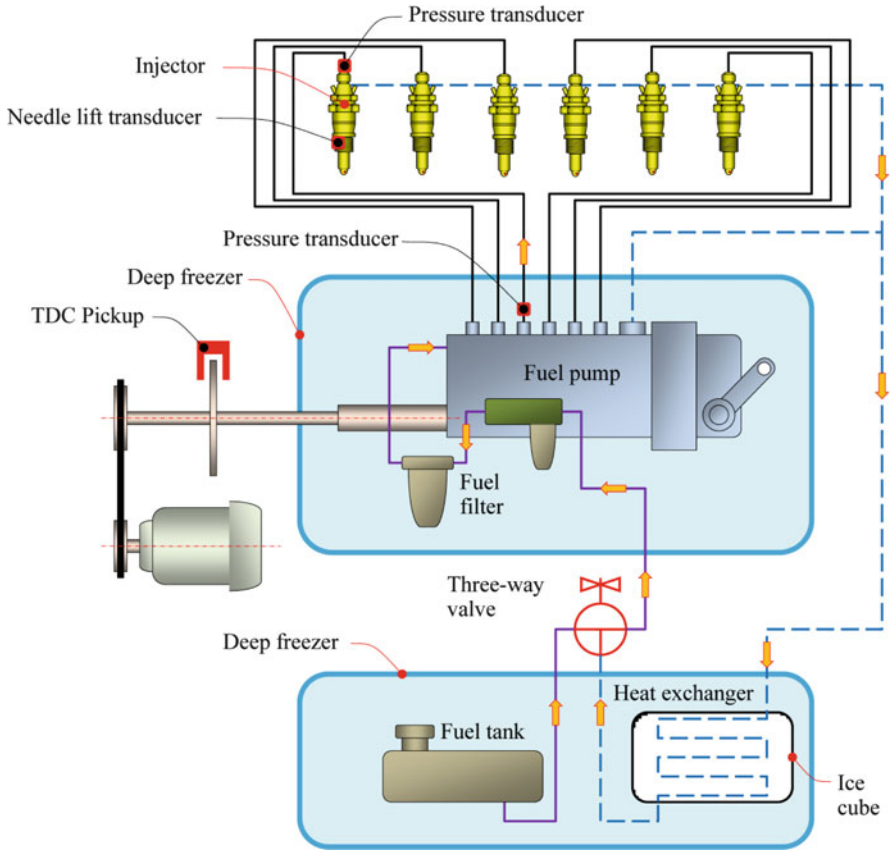


Fig. 2.17 Fuel injection system test bed for low fuel temperature measurements

fuel from the tank in a 3-way mixing valve and fed to the fuel pump. This enables an accurate fuel temperature control at the injection pump inflow.

The test bench and fuel injection system should be fully instrumented in order to measure the basic parameters, characteristic for system operation. A computer-aided measuring system should be used to acquire electric signals from applied sensors. The system incorporates a personal computer and a multifunction card. Appropriate software should be used to build the computer applications for data acquisition, data analyses, and control algorithms. These applications can be used to control the operation of the multifunction card (data acquisition, DC voltage output) and for data logging and post-processing.

Figure 2.18 illustrates the output from a typical test procedure, where p_I and p_{II} denote the measured pressures immediately after the pump and just before the injector. It is evident that the pressure before the injector delays and differs from the pressure after the pump. This is due to the compressibility of fuel, sound velocity of the fuel, spring forces, reflected pressure waves, etc. When the needle

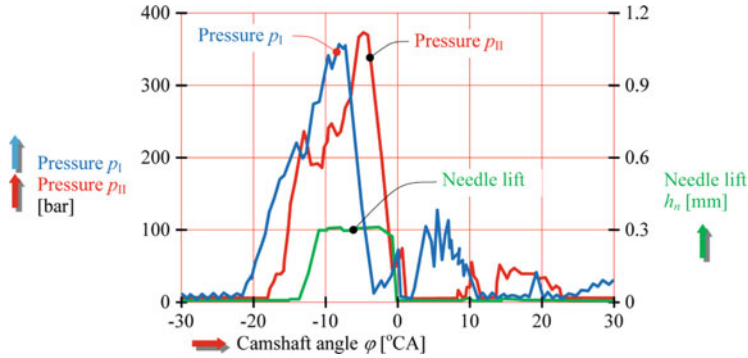


Fig. 2.18 Injection characteristics measured at the test bench

lifts, the pressure before the injector drops a little bit but starts to rise again once the injector is fully open. From the injection characteristics given in Fig. 2.18 the injection delay, injection timing, and injection duration can also be determined.

2.1.2 Mathematical Modeling and Simulation

In order to reduce the cost for experimental work, mathematical modeling of injection processes and numerical simulation may help substantially in the engine development process. Mathematical models of injection processes vary significantly in complexity, which leads to significant differences in accuracy, robustness, and computational efficiency. This book does not focus on mathematical modeling of injection processes. Therefore, only a relatively simple one-dimensional model will be presented in the following. The reason for this is that this model exhibits respectable computational efficiency, very good robustness, and quite reasonable accuracy. As such, it is also quite well suited to be employed in injection system optimization procedures.

The model (Kegl 1995) presented here simulates the injection process in a mechanically controlled in-line fuel injection system (Fig. 2.19) as a one-dimensional flow. The whole injection process is described by the following fifteen variables:

$$\text{Injection rate } q \left[\frac{\text{mm}^3}{\text{ms}} \right],$$

Pressure in the in-barrel chamber p_k [MPa],

Pressure in the delivery valve chamber p_{dv} [MPa],

Pressure in the snubber valve chamber p_{sv} [MPa],

Pressure in the injector chamber p_{in} [MPa],

Volume of vapor cavities in the delivery valve chamber V_v^{dv} [mm³],

Volume of vapor cavities in the snubber valve chamber V_v^{sv} [mm³],

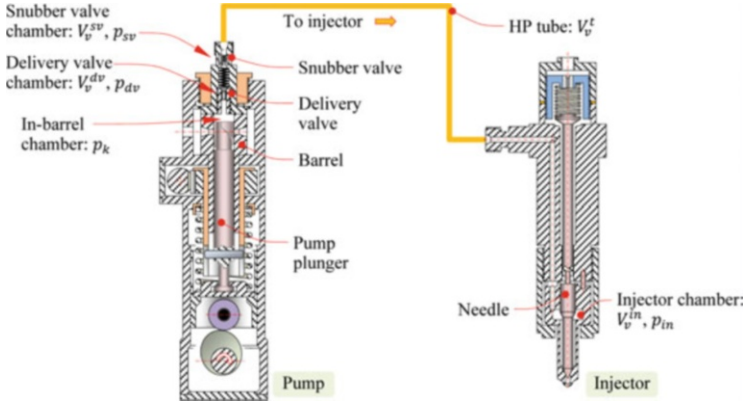


Fig. 2.19 Modeled fuel injection system

Volume of vapor cavities in the high pressure tube V_v^t [mm³],

Volume of vapor cavities in the injector chamber V_v^{in} [mm³],

Lift of the delivery valve h_{dv} [mm],

Velocity of the delivery valve v_{dv} $\left[\frac{m}{s}\right]$,

Lift of the snubber valve h_{sv} [mm],

Velocity of the snubber valve v_{sv} $\left[\frac{m}{s}\right]$,

Needle lift h_n [mm],

Needle velocity v_n $\left[\frac{m}{s}\right]$.

These quantities are related to each other and to time by a system of fifteen ordinary differential equations, involving an unknown parameter—the residual pressure p_0 . Since this quantity is not known in advance, iterations are needed to solve this system of differential equations.

All of the used equations are either *equations of continuity* or *equations of motion*. The former ones are used to express the time derivatives of the injection rate; of the pressures in the in-barrel chamber, delivery valve, snubber valve, and injector chamber; and of the volume of vapor cavities in the delivery valve, snubber valve, and injector chamber. Equations of motion are used to express the time derivatives of the lift and velocity of the delivery valve, snubber valve, and the needle.

The *injection rate* $q = dq_{inj}/dt$ is given by

$$q = (\mu_{in} A_{in}) \sqrt{\frac{2}{\rho} |p_{in} - p_a|}, \quad (2.3)$$

where q_{inj} is fuelling, $(\mu_{in} A_{in})$ denotes the actual (effective) cross-section area of the injector nozzles, ρ denotes the fuel density, p_{in} is the pressure in the injector chamber, and p_a is the pressure in the chamber into which the fuel is injected.

The time derivative of the *pressure* in the *in-barrel chamber* p_k is

$$\begin{aligned} \frac{dp_k}{dt} = & \left[A_k v_k - (\mu_p A_p) \sqrt{\frac{2}{\rho} |p_k - p_n|} \times \text{sgn}(p_k - p_n) \right. \\ & \left. - (\mu_{dv} A_{dv}) \sqrt{\frac{2}{\rho} |p_k - p_{dv}|} \times \text{sgn}(p_k - p_{dv}) - A_{dv} v_{dv} \right] \times \frac{E}{V_k} \end{aligned} \quad (2.4)$$

where E is the modulus of fuel compressibility, V_k is the volume of the in-barrel chamber, A_k is the pump plunger cross-section area, v_k is pump plunger velocity, $(\mu_p A_p)$ is the effective flow area of feed/spill ports, p_k is the pressure in the in-barrel chamber, p_n is the pressure in the pump sump, $(\mu_{dv} A_{dv})$ is the effective flow area of the delivery valve, p_{dv} is the pressure in the delivery valve chamber, A_{dv} is the cross-section area of the delivery valve, and v_{dv} denotes the delivery valve velocity.

The time derivative of the *pressure* in the *delivery valve chamber* p_{dv} is

$$\frac{dp_{dv}}{dt} = \begin{cases} \left[(\mu_{dv} A_{dv}) \sqrt{\frac{2}{\rho} |p_k - p_{dv}|} \times \text{sgn}(p_k - p_{dv}) + A_{dv} v_{dv} - \right. \\ \left. A_{sv} v_{sv} - (\mu_{sv} A_{sv}) \sqrt{\frac{2}{\rho} |p_{dv} - p_{sv}|} \times \text{sgn}(p_{dv} - p_{sv}) \right] \times \frac{E}{V_{dv}}, & V_v^{dv} = 0 \\ 0, & V_v^{dv} \neq 0 \end{cases} \quad (2.5)$$

where V_{dv} denotes the volume of the delivery valve chamber, A_{sv} is the snubber valve cross-section area, v_{sv} is the snubber valve velocity, $(\mu_{sv} A_{sv})$ is the effective flow area of the snubber valve, p_{sv} is the pressure in the snubber valve chamber, and V_v^{dv} is the volume of vapor cavities in the delivery valve chamber.

The time derivative of the *pressure* in the *snubber valve chamber* p_{sv} is

$$\frac{dp_{sv}}{dt} = \begin{cases} [A_{sv} v_{sv} + \\ (\mu_{sv} A_{sv}) \sqrt{\frac{2}{\rho} |p_{dv} - p_{sv}|} \times \text{sgn}(p_{dv} - p_{sv}) - A_t w_I] \times \frac{E}{V_{sv}}, & V_v^{sv} = 0 \\ 0, & V_v^{sv} \neq 0 \end{cases} \quad (2.6)$$

where A_t denotes the cross-section area of the high pressure tube, w_I is the flow velocity at the point I-I (Fig. 2.20), V_{sv} is the volume in the snubber valve chamber, and V_v^{sv} is the volume of vapor cavities in the snubber valve chamber.

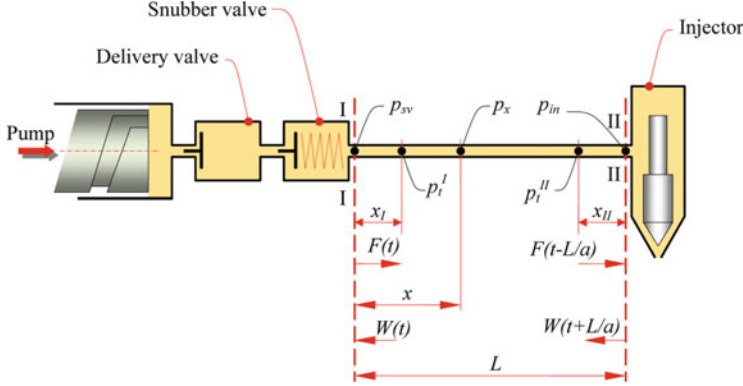


Fig. 2.20 Scheme of the in-line fuel injection system

The time derivative of the *pressure* in the *injector chamber* p_{in} is

$$\frac{dp_{in}}{dt} = \begin{cases} [A_I w_{II} - (\mu_{in} A_{in}) \sqrt{\frac{2}{\rho} |p_{in} - p_a|} \times \text{sgn}(p_{in} - p_a) - A_n^{st} v_n] & V_v^{in} = 0 \\ 0 & V_v^{in} \neq 0 \end{cases} \quad (2.7)$$

where w_{II} is the flow velocity at the point II-II (Fig. 2.20), $(\mu_{in} A_{in})$ is the effective flow area of the injector chamber, A_n^{st} is the cross-section area of the needle stem, v_n denotes needle velocity, V_{in} is the volume of the injector chamber, and V_v^{in} is the volume of vapor cavities in the injector chamber.

The time derivative of the *volume of vapor cavity* in the *delivery valve chamber* V_v^{dv} is

$$\frac{dV_v^{dv}}{dt} = \begin{cases} - \left[(\mu_{dv} A_{dv}) \sqrt{\frac{2}{\rho} |p_k - p_{dv}|} \times \text{sgn}(p_k - p_{dv}) + A_{dv} v_{dv} - A_{sv} v_{sv} - (\mu_{sv} A_{sv}) \sqrt{\frac{2}{\rho} |p_{dv} - p_{sv}|} \times \text{sgn}(p_{dv} - p_{sv}) \right] & p_{dv} = p_v \\ 0, & \text{otherwise} \end{cases} \quad (2.8)$$

where p_v denotes the evaporation pressure.

The time derivative of the *volume of vapor cavity in the snubber valve chamber* V_v^{sv} is

$$\frac{dV_v^{sv}}{dt} = \begin{cases} -[A_{sv}v_{sv} + (\mu_{sv}A_{sv})\sqrt{\frac{2}{\rho}}|p_{dv} - p_{sv}| \times \text{sgn}(p_{dv} - p_{sv}) - A_t w_1], & p_{sv} = p_v \\ 0, & \text{otherwise} \end{cases} \quad (2.9)$$

The time derivative of the *volume of vapor cavity in the high pressure tube* V_v^t is

$$\frac{dV_v^t}{dt} = (w_{II} - w_I) \times A_t, \quad (2.10)$$

where A_t denotes the cross-section area of the high pressure tube.

The time derivative of the *volume of vapor cavity in the injector chamber* V_v^{in} is

$$\frac{dV_v^{in}}{dt} = \begin{cases} -[A_t w_{II} - (\mu_{in}A_{in})\sqrt{\frac{2}{\rho}}|p_{in} - p_a| \times \text{sgn}(p_{in} - p_a) - A_n^{st}v_n], & p_{in} = p_v \\ 0, & \text{otherwise} \end{cases} \quad (2.11)$$

The time derivatives of the *lift* h_{dv} and *velocity* v_{dv} of the *delivery valve* are

$$\frac{dh_{dv}}{dt} = \begin{cases} 0, & F_{dv} \geq 0 \text{ and } h_{dv} = h_{dv}^{\max} \\ 0, & F_{dv} \leq 0 \text{ and } h_{dv} = 0 \\ v_{dv}, & \text{otherwise} \end{cases} \quad (2.12)$$

$$\frac{dv_{dv}}{dt} = \begin{cases} 0, & F_{dv} \geq 0 \text{ and } h_{dv} = h_{dv}^{\max} \\ 0, & F_{dv} \leq 0 \text{ and } h_{dv} = 0 \\ \frac{F_{dv}}{m_{dv}}, & \text{otherwise} \end{cases} \quad (2.13)$$

The time derivatives of the *lift* h_{sv} and *velocity* v_{sv} of the *snubber valve* are

$$\frac{dh_{sv}}{dt} = \begin{cases} 0, & F_{sv} \geq 0 \text{ and } h_{sv} = h_{sv}^{\max} \\ 0, & F_{sv} \leq 0 \text{ and } h_{sv} = 0 \\ v_{sv}, & \text{otherwise} \end{cases} \quad (2.14)$$

$$\frac{dv_{sv}}{dt} = \begin{cases} 0, & F_{sv} \geq 0 \text{ and } h_{sv} = h_{sv}^{\max} \\ 0, & F_{sv} \leq 0 \text{ and } h_{sv} = 0 \\ \frac{F_{sv}}{m_{sv}}, & \text{otherwise} \end{cases} \quad (2.15)$$

where $F_{dv} = A_{dv} \times (p_k - p_{dv}) - F_0^{dv} - C_{dv}h_{dv}$ represents the sum of forces, which act on the delivery valve, h_{dv} denotes the delivery valve lift, h_{dv}^{\max} is the maximum delivery valve lift, m_{dv} is the mass of delivery valve moving parts, F_0^{dv} is the preload spring force, and C_{dv} is the delivery valve spring stiffness, $F_{sv} = A_{sv} \times (p_{dv} - p_{sv}) - F_0^{sv} - C_{sv}h_{sv}$ represents the sum of forces, which act on the snubber valve, h_{sv} denotes the snubber valve lift, h_{sv}^{\max} is the maximum snubber valve lift, m_{sv} is the mass of snubber valve moving parts, F_0^{sv} is the preload spring force, and C_{sv} is the snubber valve spring stiffness. The movement of the delivery valve is limited to the interval $[0, h_{dv}^{\max}]$ and the movement of the snubber valve is limited to the interval $[0, h_{sv}^{\max}]$.

The time derivatives of the *needle lift* h_n and *velocity* v_n are

$$\frac{dh_n}{dt} = \begin{cases} 0, & F_n \geq 0 \text{ and } h_n = h_n^{\max} \\ 0, & F_n \leq 0 \text{ and } h_n = 0 \\ v_n, & \text{otherwise} \end{cases} \quad (2.16)$$

$$\frac{dv_n}{dt} = \begin{cases} 0, & F_n \geq 0 \text{ and } h_n = h_n^{\max} \\ 0, & F_n \leq 0 \text{ and } h_n = 0 \\ \frac{F_n}{m_{in}}, & \text{otherwise} \end{cases} \quad (2.17)$$

where $F_n = (A_n^{\text{st}} - A_n^{\text{se}}) \times p_{in} + A_n^{\text{se}} \times p_{\text{sac}} - F_0^n - C_n h_n$ represents the sum of forces, which act on the needle, A_n^{se} is the cross-section area of the needle seat, p_{sac} is the pressure in the sac volume, h_n denotes the needle lift, h_n^{\max} is the maximum needle lift, m_{in} is the mass of injector moving parts, F_0^n is the preload spring force, and C_n is the needle spring stiffness. The movement of needle is limited to the interval $[0, h_n^{\max}]$.

The *pressure in the sac volume* p_{sac} is given by

$$p_{\text{sac}} = \frac{K^2}{1 + K^2} \times (p_{in} - p_a) + p_a, \quad (2.18)$$

where $K = \frac{(\mu_{in} A_{in})}{(\mu_{in} A_{in})_{\max}}$.

In general, to determine the velocities w_I and w_{II} in the high pressure tube and to relate them to pressure waves (Fig. 2.20), the equations of momentum and continuity are used:

$$\frac{\partial p}{\partial x} + \rho \frac{\partial w}{\partial t} + \rho k w = 0, \quad (2.19)$$

$$\frac{\partial w}{\partial x} + \frac{1}{a^2 \rho} \times \frac{\partial p}{\partial t} = 0, \quad (2.20)$$

where ρ denotes the fuel density, k is the resistance factor, w is fuel velocity, a is the sound velocity, t is time, and x is a coordinate, measured along the HP tube.

By integrating these two equations, the pressure and velocity at x coordinate can be expressed as follows:

$$p_x = p_0 + F\left(t - \frac{x}{a}\right) \times e^{-\frac{kx}{a}} - W\left(t + \frac{x}{a}\right) \times e^{-\frac{k(L-x)}{a}}, \quad (2.21)$$

$$w_x = \frac{1}{a\rho} \times \left[F\left(t - \frac{x}{a}\right) \times e^{-\frac{kx}{a}} + W\left(t + \frac{x}{a}\right) \times e^{-\frac{k(L-x)}{a}} \right], \quad (2.22)$$

where L is the length of the high pressure tube, a denotes the sound velocity in the fluid, and p_0 is the residual pressure in the high pressure system between two injections. The function F denotes the forward pressure wave, traveling from I-I to II-II (Fig. 2.20). The function W denotes the reflected pressure wave. Both pressure wave functions are defined later in the text. The pressures at the I-I and II-II cross section in the high pressure tube are marked as p_I^I and p_I^{II} . The numerical determination of the pressure at monitoring points I-I and II-II is necessary in order to verify the mathematical model with experiment.

The *resistance factor* k is derived on the basis of experimental work (Kegl 1995). Based on experimental data, ad hoc formulas for the determination of k can be developed. Typical parameters in these formulas are engine speed n , tube diameter d_t , tube length L , and maximum value of effective flow area of the injector chamber, for example,

$$k = 4.5 \times (60.36 + 3n) \times \left(\frac{0.002}{d_t}\right)^{2.75} \times \left(\frac{(\mu_{in}A_{in})_{max}}{4.272 \times 10^{-7}}\right)^{0.72} \times \left(\frac{0.5}{L}\right)^{0.8633}. \quad (2.23)$$

The forward pressure wave and fuel velocity at cross-section I-I can be expressed as

$$F(t) = p_{sv} - p_0 + W(t) \times e^{-\frac{kL}{a}}, \quad (2.24)$$

$$w_I = \frac{1}{a\rho} \times \left(p_{sv} - p_0 + 2W(t) \times e^{-\frac{kL}{a}} \right), \quad (2.25)$$

and the reflected pressure wave and fuel velocity at cross-section II-II as

$$W\left(t + \frac{L}{a}\right) = p_0 - p_{in} + F\left(t - \frac{L}{a}\right) \times e^{-\frac{kL}{a}}, \quad (2.26)$$

$$w_{II} = \frac{1}{a\rho} \times \left(p_0 - p_{in} + F \left(t - \frac{L}{a} \right) \times e^{-\frac{kt}{a}} \right). \quad (2.27)$$

The *residual pressure* p_0 can be expressed in dependence on the delivery and snubber valve parameters as follows:

$$p_0 = p_{s(h_n=0)} - \frac{A_{dv} h_{dv(h_n=0)} E}{V_s}, \quad (2.28)$$

where $h_{dv(h_n=0)}$ is the delivery valve lift and $p_{s(h_n=0)}$ is the pressure in the high pressure system at the time when the needle closes ($h_n = 0$). Due to the presence of the snubber valve,

$p_{s(h_n=0)}$ can be calculated as

$$p_{s(h_n=0)} = \frac{\sum_{i=1}^m p_t^{z_i} + p_{dv} + p_{sv} + p_{in}}{m + 3}, \quad (2.29)$$

where the quantities $p_t^{z_i}, i = 1 \dots m$ represent the pressures in the high pressure tube, calculated at m equidistant points, each point being positioned at the distance z_i , measured from the cross-section I-I. The pressure $p_t^{z_i}$ can be expressed as

$$p_t^{z_i} = p_0 + F \left(t - \frac{z_i}{a} \right) \times e^{-\frac{kz_i}{a}} - W \left(t + \frac{L - z_i}{a} \right) \times e^{-\frac{k(L-z_i)}{a}}, i = 1 \dots m. \quad (2.30)$$

On the basis of the residual pressure p_0 and evaporation pressure p_v , the total volume of vapor cavities in the high pressure system, at the beginning of injection, can be calculated as

$$V_v^0 = \begin{cases} \frac{V_s}{E} (p_v - p_0), & p_v > p_0 \\ 0, & p_v \leq p_0 \end{cases} \quad (2.31)$$

Furthermore, it can be assumed that initially the vapor in the system is distributed proportionally to the system dead volumes. Therefore, it follows that the initial vapor volumes in the delivery valve chamber $V_v^{dv,0}$, snubber valve chamber $V_v^{sv,0}$, high pressure tube $V_v^{t,0}$, and injector chamber $V_v^{in,0}$ are as follows:

$$V_v^{dv,0} = \frac{V_{dv}}{V_s} V_v^0, \quad V_v^{sv,0} = \frac{V_{sv}}{V_s} V_v^0, \quad V_v^{t,0} = \frac{V_t}{V_s} V_v^0, \quad V_v^{in,0} = \frac{V_{in}}{V_s} V_v^0. \quad (2.32)$$

In dependence on instantaneous vapor volume, pressure, and temperature, the instant values of fuel density, modulus of compressibility, and sound velocity can be computed (Kegl 1995, 2006).

The presented system of 15 first-order ordinary differential equations for the simulation of fuel injection process could be integrated straightforwardly by using any standard method, if the residual pressure would be known a priori. Since this is not the case, iterations are required starting with an assumed value of the residual pressure. In the first iteration, time integration can be done with an estimated residual pressure, being somewhat higher than the evaporation pressure. After the first integration is completed, the new residual pressure is calculated as discussed in the text. This value is then used as an estimation of the residual pressure for the next iteration and so on. The procedure is terminated when the difference of the calculated residual pressure in two successive iterations is smaller than some prescribed value (Kegl 1995).

The model presented in this section was implemented in a software package named BKIN. Therefore the term BKIN will be used throughout this book to reference this model.

2.2 Fuel Spray Characteristics

The most important diesel fuel spray characteristics may be classified as

- *Macroscopic quantities* such as:
 - Spray tip penetration
 - Cone angle
- *Microscopic quantities* such as:
 - Droplet size

All fuel spray characteristics (Fig. 2.21) influence the combustion process and consequently the economy and ecology characteristics and engine performance (Hiroyasu and Arai 1990; Kegl 2004; Soid and Zainal 2011).

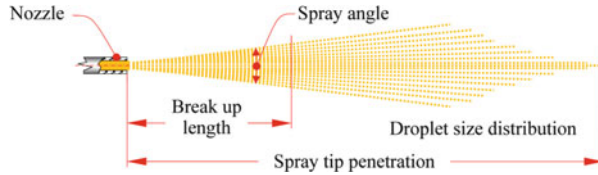
Fuel spray tip penetration L_p is defined as the maximal distance measured from the injector to the spray tip. It represents the maximum penetration length achieved by the droplets in the center of the spray.

Spray cone angle θ is defined as the angle between two straight lines originating from the orifice exit of the nozzle and being tangent to the spray outline. This angle usually ranges from 5 to 30°.

Droplet size is usually measured on an average basis by the *medium diameter of the droplets* d_{32} , called the Sauter mean diameter. This quantity can be used to estimate the quality of atomization of the fuel.

Fuel spray penetration is determined by the equilibrium of two factors: the linear momentum of the injected fuel and the resistance of the working fluid (either gas or liquid) in the control volume. Due to friction, the kinetic energy of the fuel is transferred progressively to the working fluid. This energy transfer decreases continuously the kinetic energy of the droplets until their movement depends solely

Fig. 2.21 Fuel spray characteristics



on the movement of the working fluid. Several studies show that spray penetration overcomes that of a single droplet. This is because the front droplets accelerate the surrounding fluid, causing the following droplets to have less aerodynamic resistance (Hiroyasu and Arai 1990; Gao et al. 2009a, b). One must emphasize that diesel fuel sprays tend to be of a compact type, which causes them to have large penetrations.

Diesel fuel spray penetration depends to a great extent on injection pressure, fuel properties, and nozzle geometry.

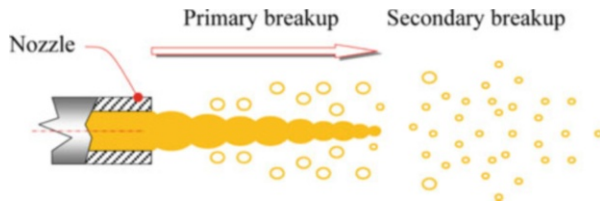
By increasing the injection pressure the fuel penetration velocity is increased. This means increased fuel momentum and larger spray penetration. Fuel properties like density, viscosity, and surface tension also affect spray penetration significantly. However, when making raw estimates, fuel density is often used as the only influencing property. In this context it is worth noting that fuel density of a given fuel may vary, for example, due to variations in fuel temperature. An increase of fuel temperature typically reduces the fuel density, which results in shorter spray penetration (Hiroyasu and Arai 1990; Gao et al. 2009a, b).

The *cone angle* is mainly affected by the geometric characteristics of the nozzle, the fuel and air density, and the Reynolds number of the fuel. Furthermore, the cone angle increases by increasing the injection pressure and by decreasing the working fluid temperature (Desantes et al. 2006; Hiroyasu and Arai 1990).

The *diameters of the droplets* depend on injection pressure, on working fluid temperature, and on fuel properties (Pogorevc et al. 2008; Desantes et al. 2006; Zhang et al. 2012). The diameters of the droplets tend to become smaller as the injection pressure raises. Furthermore, the working fluid temperature and fuel properties influence the evaporation rate, which also affects the droplet size. Namely, by increasing the temperature the rate of evaporation increases. Consequently, the droplets with small diameters tend to evaporate completely within a quite short time interval. On the other side, the droplets with greater diameters maintain a stable geometry for some time until they also evaporate completely.

In a fuel spray, fuel droplets evaporate as they travel away from the nozzle. The maximal distance, reached by the droplets before they all evaporate, is called the *liquid length*. After the liquid length is reached, the evaporated fuel continues to penetrate the surrounding gas and its range is denoted as the *vapor length*. It was found out that the liquid length tends to stabilize after a short spray development time and then remains approximately constant. On the other hand, in a typical diesel injection timeframe (a few milliseconds) the vapor length does not reach a steady state.

Fig. 2.22 Fuel spray breakup



Liquid spray formation is a rather sophisticated physical process, starting from the breakup of the liquid core into droplets, shortly after the nozzle exit, called the *primary breakup*. In the second stage the *formed droplets break up into smaller droplets*, which is called the *secondary breakup* (Fig. 2.22).

2.2.1 Experimental Techniques

The techniques used in the past for droplet size measurement can be classified into *mechanical methods* (droplet capture, cascade impaction, frozen drop and wax methods, and sedimentation technique), *electrical methods* (Wickse Dukler technique, the charged wire probe, and the hot wire anemometer), and *optical methods* (photography, holography, laser diffraction, laser anemometry, and various other techniques based on light scattering) (Soid and Zainal 2011; Leng et al. 2010; Myong et al. 2008; Andreassi et al. 2007; Payri et al. 2005). *Optical techniques* were commonly used for macroscopic and microscopic fuel sprays and combustion characterization. However, these techniques can often be difficult to implement and they are relatively expensive.

The macroscopic parameters such as the *cone angle* and the *tip penetration* can be determined through *direct visualization methods* (Fig. 2.23), where diesel spray injection can be studied in a high pressure and temperature cell. Spray propagation can be followed by using, for example, two intensified charge-coupled device cameras with double framing options. Two-dimensional flash light shadowgraph, laser elastic scattering, and chemiluminescence can be used to investigate the fuel propagation (Soid and Zainal 2011; Payri et al. 2005; Myong et al. 2008).

The microscopic parameters such as the *droplet size* can nowadays be measured by using either *PIV* or *PDPA techniques*. Figure 2.24 shows the experimental apparatus for the LIF-PIV experiment (Soid and Zainal 2011; Moon et al. 2010; Andreassi et al. 2007). A double pulsed Nd:YAG laser is utilized to obtain the fluoresced images of tracer droplets. A light sheet is generated using a sheet generator equipped with a cylindrical lens inside it. When the tracer droplets are fluoresced by the laser light, images are captured by a charge-coupled device (CCD) camera. A long-pass filter, which transmits the wavelengths longer than 560 nm, has to be installed in front of the CCD camera to capture the fluoresced signal of the tracer droplets. The pressures inside the constant volume vessel and the tracer reservoir can be controlled by pressure regulators. Two delay generators

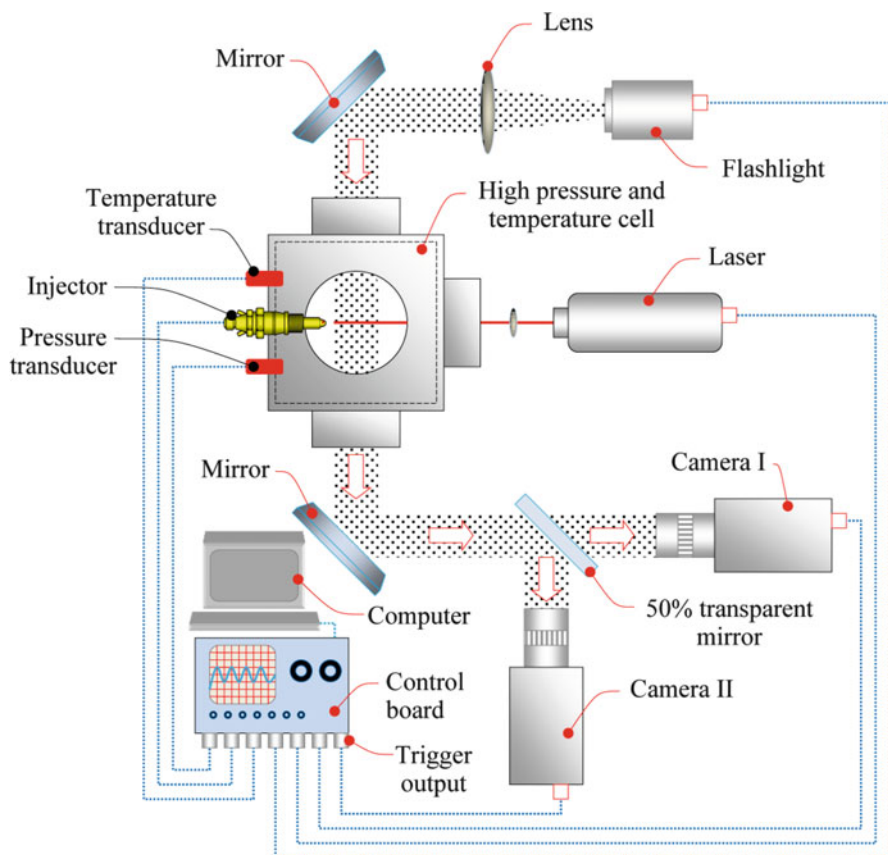


Fig. 2.23 Spray visualization setup

have to be employed to synchronize the tracer injection, fuel injection, laser firing, and image capturing timings. The image capturing timing and exposure time are determined by the laser shot timings and shot durations.

2.2.2 Mathematical Modeling and Simulation

Diesel fuel sprays have always been a challenge for fluid modelers since these sprays typically consist of a very large number of droplets. Each droplet has unique properties and is subject to complex interactions that are a function of those properties. Till now, most of the strategies, which were formulated over the years to address this problem, fall into *Eulerian–Eulerian* or *Eulerian–Lagrangian* type formulations.

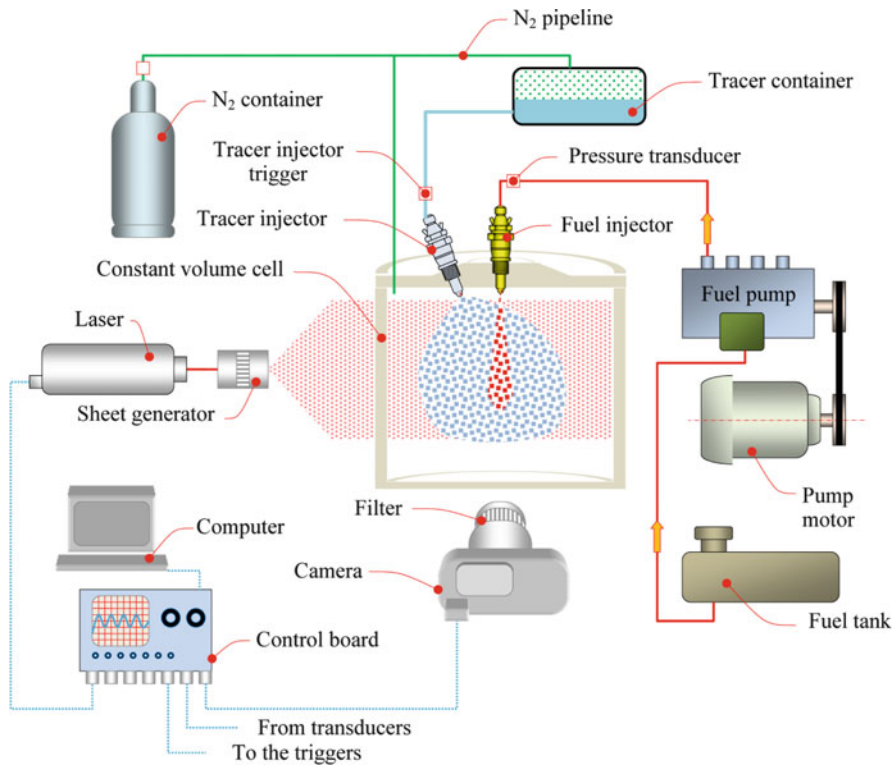


Fig. 2.24 Experimental apparatus for LIF-PIV

The *Eulerian–Eulerian* formulation uses for the spray a two-fluid model and solves the Eulerian field equations for both the liquid and the gaseous phase in order to obtain the liquid phase penetration. In the literature, the relative simplicity and grid independence are often listed as the main advantages of this approach. However, this approach cannot model easily the interaction between phases. Furthermore, the gas and the liquid velocities are assumed to be the same and the turbulence in the liquid phase is assumed to follow the gas phase turbulence (Iyer et al. 2002; Tatschl et al. 2002; Gidaspow 1994).

The *Eulerian–Lagrangian* formulation uses the Lagrangian approach for the liquid phase by modeling droplets as discrete particles. The positions of these particles are tracked in space and time by solving the Newton's equations of motion. The gaseous phase is treated in an Eulerian manner. In the literature, relative easy modeling of the interaction between phases by using sub-models for atomization, drop dispersion, collision, coalescence, breakup, and vaporization are often listed as the main advantages of this approach. The limitations are related to grid dependence, computational time, and memory requirements (Dukowicz 1980; Sazhina et al. 2000).

Currently, the most common Eulerian–Lagrangian description is based on the *Lagrangian discrete droplet method* (Tatschl et al. 2002; Dukowicz 1980). While the continuous gaseous phase is described by the standard Eulerian conservation equations, the transport of the dispersed phase is calculated by tracking the trajectories of a certain number of representative computational particles, called parcels. A parcel consists of a number of droplets and it is assumed that all the droplets within one parcel have the same physical properties and behave equally when they move, break up, hit a wall, or evaporate. The coupling between the liquid and the gaseous phases is achieved by the source term exchange for mass, momentum, energy, and turbulence. Various sub-models account for the effects of turbulent dispersion (Gosman and Ioannides 1983), coalescence (O'Rourke 1980), evaporation (Dukowicz 1979), wall interaction (Naber and Reitz 1988), and droplet breakup (Liu and Reitz 1993).

Among all phenomena related to spray development, such as *evaporation* or *droplet collision*, the *breakup process* is clearly recognized as the most important and still today has not been fully solved (Battistoni and Grimaldi 2012; Lee and Park 2002; Pogorevc et al. 2008). In practical implementation, droplet breakup rate is commonly approached through the velocity of loss of droplet radius r_d , expressed as

$$\frac{dr_d}{dt} = \frac{r_d - r_s}{t_b}, \quad (2.33)$$

where r_s is a the stable radius and t_b is the characteristic breakup time.

Due to the very high injection pressures in diesel engines, it is not recommendable to uniformly handle the whole breakup process. Therefore, breakup phenomena occurring near the nozzle exit, where the initial liquid column is disintegrated into ligaments or droplets, are accounted for by *primary breakup* models, whereas prediction of further breakup process, starting from initial drops, is handled by *secondary breakup* models (Fig. 2.25) (Battistoni and Grimaldi 2012; Lee and Park 2002; Pogorevc et al. 2008).

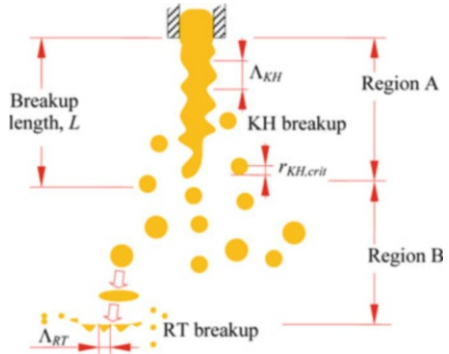
In the KH–RT hybrid model, it is assumed that primary breakup mainly occurs by KH instability while RT instability causes the secondary breakup as shown in Fig. 2.25. In region A, a droplet is detached from the intact liquid core by the KH instability. Once the droplet is detached from the intact sheet, the secondary breakup occurs by the competing KH and RT instabilities in the region B.

The *primary diesel breakup model* (KH model—Kelvin–Helmholtz model) is based on the rate approach and aims at capturing the combination of the aerodynamic mechanism, modeled through the wave approach, and the turbulence mechanism with included cavitation effects. The liquid breakup length L , (Fig. 2.25) is calculated by

$$L = C_3 \times d_{nh} \times We^{0.32}, \quad (2.34)$$

where C_3 is the constant, d_{nh} is the nozzle hole diameter, and We is the Weber number of the fuel.

Fig. 2.25 Primary and secondary breakup models



During the breakup, the droplet radius r_d reduces to the critical radius $r_{KH,crit}$ with uniform rate. In this case, the critical droplet radius $r_{KH,crit}$ and the primary breakup time t_{KH} are given by

$$\begin{aligned} r_{KH,crit} &= C_1 \times \Lambda_{KH} \quad \Lambda_{KH} = \Lambda_{KH}(r_d, Z, T, We) \\ t_{KH} &= \frac{3.726 \times C_2 \times r_d}{\Lambda_{KH} \times \Omega_{KH}} \quad \Omega_{KH} = \Omega_{KH}(r_d, Z, T, We, \sigma, \rho_f) \end{aligned} \quad (2.35)$$

where C_1 and C_2 are the primary breakup model constants, Ω_{KH} and Λ_{KH} are the frequency and the corresponding wavelength of the fastest growing KH wave, r_d is the droplet radius, ρ_f is the fuel density, σ_f is the fuel surface tension, Z is the Ohnesorge number, T is the Taylor number, and Re is the Reynolds number:

$$\begin{aligned} We &= \frac{\rho_a \times r_d \times v_{rel}^2}{\sigma_f}, \\ T &= Z\sqrt{We}, \\ Z &= \frac{\sqrt{We}}{Re}, \\ Re &= \frac{\rho_f}{\mu_f} \times r_d \times v_{rel}. \end{aligned} \quad (2.36)$$

Here, v_{rel} is the relative velocity between the droplet and ambient gas, μ_f is the fuel viscosity, and ρ_a is the ambient gas density.

Because the primary breakup occurs with uniform radius reduction rate, the new droplet radius r_{new} can be calculated as

$$\frac{r_d - r_{new}}{dt} = \frac{r_d - r_{KH,crit}}{t_{KH}}. \quad (2.37)$$

The *secondary diesel breakup model* (RT model—Rayleigh–Taylor model) is based on the wave model. Here, the initial size of the droplet diameter is supposed

to be equal to the wavelength of the fastest growing or most probable unstable surface wave. The wavelength Λ_{RT} of the fastest growing wave can be calculated as

$$\Lambda_{RT} = \frac{C_4}{K_{RT}} K_{RT} = K_{RT}(\rho_a, \rho_f, \sigma_f, g, a), \quad (2.38)$$

where C_4 is a secondary breakup model constant, K_{RT} is the wave number, and g and a are the accelerations in the direction of travel due to gravity and drag force, respectively. If the waves are growing longer than the breakup time t_{RT} , the droplet is split into small droplets with radius $r_{RT,crit}$. In the secondary breakup, t_{RT} and $r_{RT,crit}$ are defined by

$$\begin{aligned} r_{RT,crit} &= \frac{C_4}{K_{RT}}, \\ t_{RT} &= \frac{C_5}{\Omega_{RT}} \Omega_{RT} = \Omega_{RT}(\rho_a, \rho_f, \sigma_f, g, a), \end{aligned} \quad (2.39)$$

where C_5 is a secondary breakup model constant, and Ω_{RT} is the frequency of fastest growing wave.

Usually, the fuel injected into the cylinder is initially assumed to form a liquid column that travels at a speed equal to the fuel injection speed until the fuel breakup time elapses. If one assumes that the flow through each nozzle is quasi-steady, incompressible, and one dimensional, the mass flow rate \dot{m}_{inj} of fuel injected through the nozzle is given by (Rad et al. 2010; Heywood 1988):

$$\dot{m}_{inj} = C_D A_n \sqrt{2\rho_f \Delta p}, \quad (2.40)$$

where C_D is the discharge coefficient, A_n is the needle cross section area, ρ_f is fuel density, and Δp is the pressure difference between injection pressure p_{inj} and ambient pressure p_a (in-cylinder pressure).

For the conditions in which no cavitation occurs, the discharge coefficient C_D can be calculated from

$$C_D = \frac{1}{\sqrt{C_i + f \frac{l_{nh}}{d_{nh}} + 1}}, \quad (2.41)$$

where c_i is the inlet loss coefficient, f is the friction coefficient, l_{nh} is the nozzle length, and d_{nh} is nozzle hole diameter. The friction coefficient can be calculated as

$$f = 0.3164 \times Re^{-0.25}. \quad (2.42)$$

Under the conditions with cavitation, the discharge coefficient C_D should be computed as

$$C_D = \sqrt{\frac{K}{2.6874 - 11.4 \frac{r_{nh}}{d_{nh}}}}, \quad (2.43)$$

where r_{nh} is the nozzle filet radius and K is the cavitation number, calculated as

$$K = \frac{p_{inj} - p_v}{\Delta p}, \quad (2.44)$$

where p_v is the saturated vapor pressure of the fuel.

Spray characteristics can also be calculated by using more or less empirical equations, developed from the experimental results. In this way, the first estimate of the fuel spray can be obtained.

Spray penetration before breakup can be calculated as (Rad et al. 2010; Heywood 1988):

$$L_p = v_{inj} t \quad 0 < t < t_b, \quad (2.45)$$

where t_b is the breakup time and the fuel injection velocity v_{inj} at the nozzle tip can be expressed as

$$v_{inj} = C_D \sqrt{\frac{2\Delta p}{\rho_f}}. \quad (2.46)$$

The *spray penetration after breakup* can be obtained as

$$L_p = 2.95 \sqrt{\left(\frac{\Delta p}{\rho_a}\right)^{0.5}} d_{nh} t \quad t \geq t_b, \quad (2.47)$$

where ρ_a is the air density.

The breakup time can be calculated as

$$t_b = 4.351 \frac{\rho_f d_{nh}}{C_D^2 \sqrt{\rho_a \Delta p}}. \quad (2.48)$$

The *spray penetration length* L_p can also be estimated independently of the breakup time by the Lustgarten equation as (Kegl et al. 2008):

$$L_p = 2 \times d_{nh}^{0.46} \times \left(\sqrt{\frac{2}{\rho_f} (p_{inj} - p_a)} \right)^{0.54} \times \left(\frac{\rho_f}{\rho_a} \right)^{0.23} \times t^{0.54}. \quad (2.49)$$

The *spray angle* can be obtained as (Rad et al. 2010; Heywood 1988):

$$\theta = \tan^{-1} \left(\frac{4\pi \left(\sqrt{\frac{3\rho_a}{\rho_f}} \right)}{18 + 1.68 \frac{I_{nh}}{d_{nh}}} \right). \quad (2.50)$$

The *droplet size distribution* within a particular range is usually expressed in terms of the *Sauter mean diameter* d_{32} . The Sauter mean diameter is defined as the volume of the droplet divided by its surface area. It can be computed by using the following empirical formulas (Rad et al. 2010; Heywood 1988):

$$d_{32} = \max(d_{32,LS}; d_{32,HS}), \quad (2.51)$$

$$\frac{d_{32,LS}}{d_{nh}} = 4.12 Re^{0.12} We^{-0.75} \left(\frac{\mu_f}{\mu_a} \right)^{0.54} \left(\frac{\rho_f}{\rho_a} \right)^{0.18}, \quad (2.52)$$

$$\frac{d_{32,HS}}{d_{nh}} = 0.38 Re^{0.12} We^{-0.75} \left(\frac{\mu_f}{\mu_a} \right)^{0.37} \left(\frac{\rho_f}{\rho_a} \right)^{-0.47}, \quad (2.53)$$

where μ_f is the dynamic viscosity of fuel, μ_a is the dynamic viscosity of air, Re the Reynolds number, and We the Weber number. Furthermore, d_{32} can also be estimated by many other simplified expressions. One of these is the well-known Hiroyasu and Kadota formula (Aigal 2003; Kegl et al. 2008):

$$d_{32} = 2.39 \times 10^3 (p_{inj} - p_a)^{-0.135} \times \rho_a \times q_{inj}^{0.131}, \quad (2.54)$$

where q_{inj} [$\text{mm}^3/\text{stroke}$] is the fuelling.

The number of drops in a particular zone can be determined, if the d_{32} and the mass of injected fuel are known. Using an energy and mass balance for a single droplet in each zone, ordinary differential equations can be set up for the rate of change of the droplet temperature and diameter, which can be subsequently solved using a suitable numerical method.

2.3 Engine Performance, Ecology, and Economy Characteristics

Among all engine performances, the *engine power* and *engine torque* are the most important. The most important ecology characteristics are related to all *harmful emissions*, such as NO_x , CO, unburned hydrocarbons (HC), particulate materials (PM), smoke, and noise. Among the economy characteristics the *specific fuel consumption* and various *tribology parameters* related to wear, deposits, and lubrication phenomena will be considered.

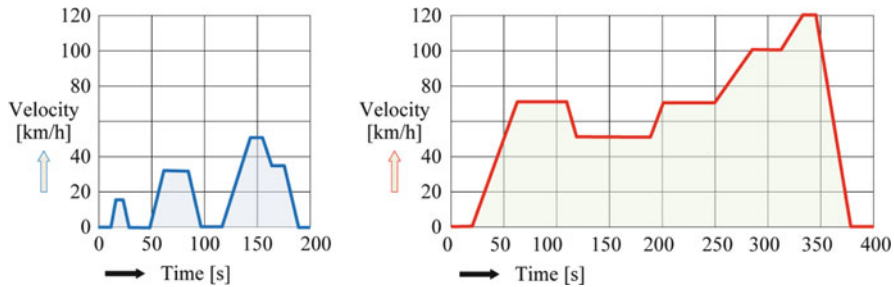


Fig. 2.26 ECE + EUDC test

2.3.1 Experimental Techniques

Nowadays, the experimental techniques related to engine power and torque are very well established and can be regarded as relatively straightforward. Therefore, in this chapter emphasis will be put onto experimental techniques related to ecology and economy.

In order to determine engine ecology characteristics, an engine is typically run under several prescribed operating conditions, termed the *engine cycle*. In practice, various steady-state and transient engine cycles are used. For example, a *transient test cycle FTP-75* for cars and light duty trucks is used for emission certification testing of cars and light duty trucks in the USA. In Japan, the urban *driving cycle JC08* is used for emission and fuel economy measurements of light duty vehicles. Furthermore, a combined *chassis dynamometer test ECE+EUDC* (Fig. 2.26) is used for emission certification of light duty vehicles (passenger cars and light commercial vehicles) in Europe.

In *transient testing* (Fig. 2.27), a constant volume sampling system is typically used to obtain the mass emission of exhaust gas components. A constant volume sampling system dilutes the entire exhaust gas with clean air to produce a constant flow. A fixed proportion of the entire diluted exhaust gas is collected in a sample bag to obtain a diluted exhaust gas that is representative for the average concentration while the engine runs. The diluted exhaust gas can also be measured continuously to obtain the average concentration during run. Mass emissions of exhaust components are obtained from the entire diluted exhaust gas flow and the average concentrations of the pollutant in the diluted gas.

A steady-state test ESC cycle for truck and bus engines is used for emission certification of heavy duty diesel engines in Europe. In the *steady-state test ESC cycle*, the importance of an individual operation mode is determined by the corresponding weighting factor. The weighting factors for all modes in percent are given in Fig. 2.28.

In *steady-state testing* (Fig. 2.29), the exhaust gas from the engine is directly collected without dilution. The mass emissions of the pollutants are obtained during the test from the quantity of exhaust gas flow, which is obtained from the air intake

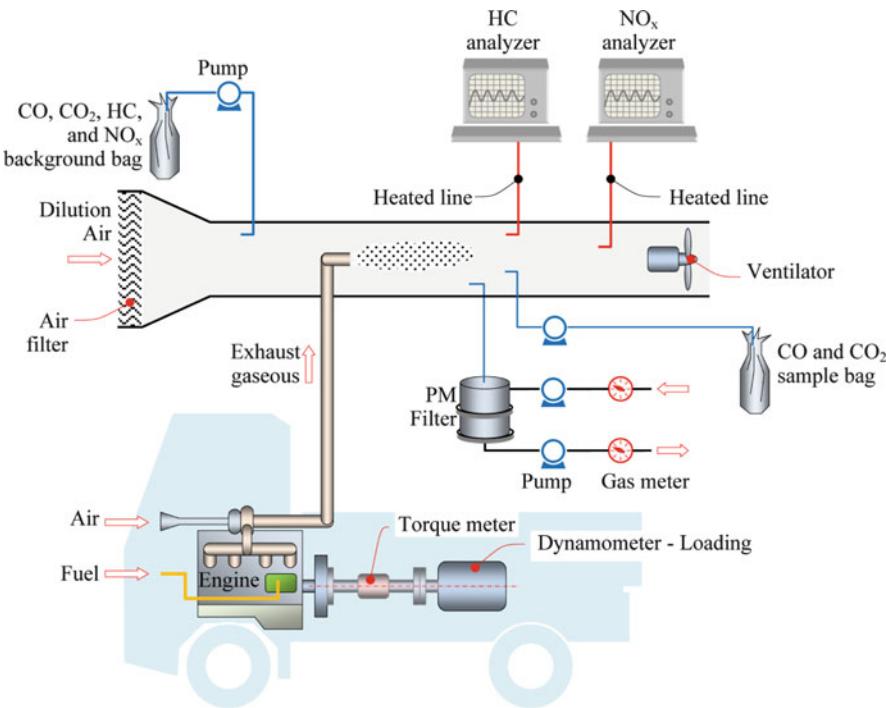


Fig. 2.27 System configuration for engine transient testing

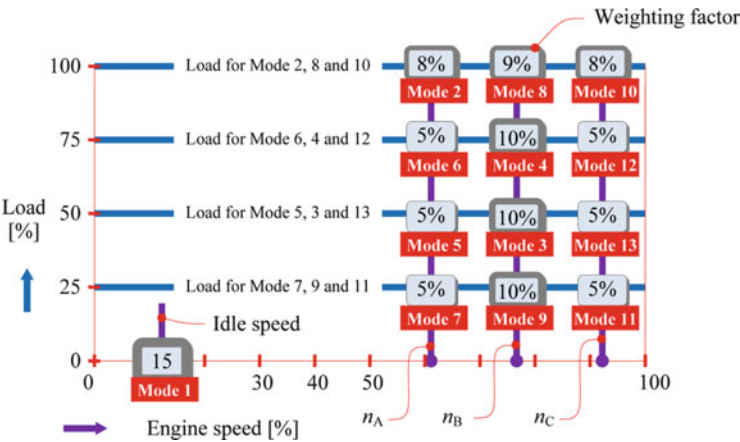


Fig. 2.28 ESC test, 13 mode cycle, weighting factors

flow and fuel flow, and the average concentrations of exhaust gas components. Because this direct measurement does not dilute the exhaust gas, this method is better than dilution measurements for measuring low concentration exhaust components.

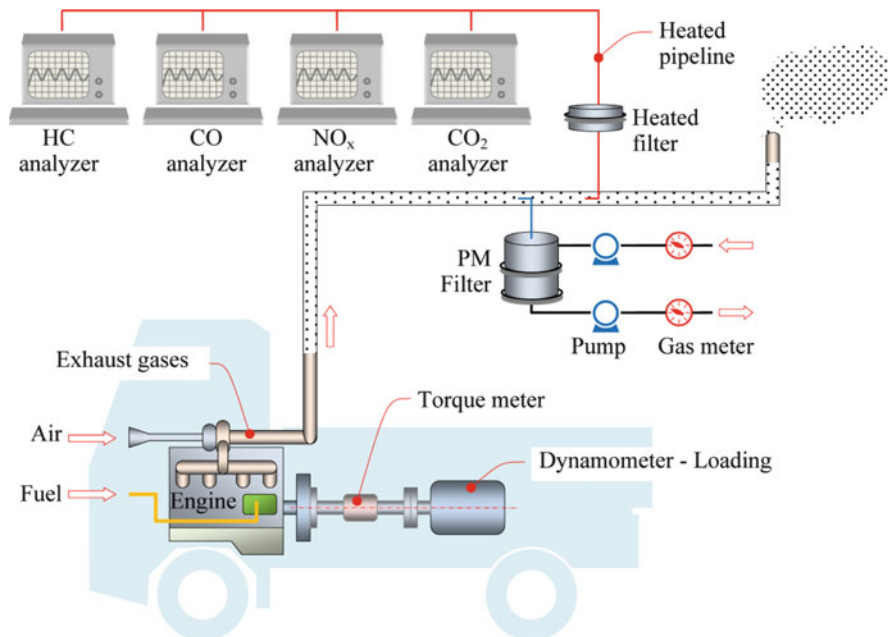


Fig. 2.29 System configuration of engine steady-state testing

A schematic diagram of the *engine test bed* is presented in Fig. 2.30 (Kegl 2008). The engine test bed consists of an engine and dynamometer, air flow rate meter, fuel consumption dynamic measuring system, analyzers of HC, NO_x, O₂, and CO, and smoke meter. By using a data acquisition system, the instantaneous pressure in the fuel high pressure tube, the instantaneous pressure in the cylinder, and the temperatures of fuel, ambient air, intake air, cooling water at inflow and outflow of the engine, oil, and exhaust gases are measured also (Fig. 2.30).

Adequate software has to be used to build the computer applications for data acquisition, data analyses, and control algorithms. These applications are used to control the operation of the data acquisition and for data logging and post-processing.

The usual techniques of emissions analysis are presented in Table 2.1 (Plint and Martyr 1995).

The *engine tribology characteristics* can be investigated by examining pump plunger surface, carbon deposits on injector and in combustion chamber, and nozzle discharge coefficient (Pehan et al. 2009). The *fuel lubrication* ability can be investigated by examining the alterations in pump plunger surfaces by using an electron microscope and by examining the *roughness parameters*. The *carbon deposits* in the combustion chambers can be examined using *endoscopic inspection*. The *deposits* in the *injector nozzle hole* can be estimated indirectly through *discharge coefficient* measurements.

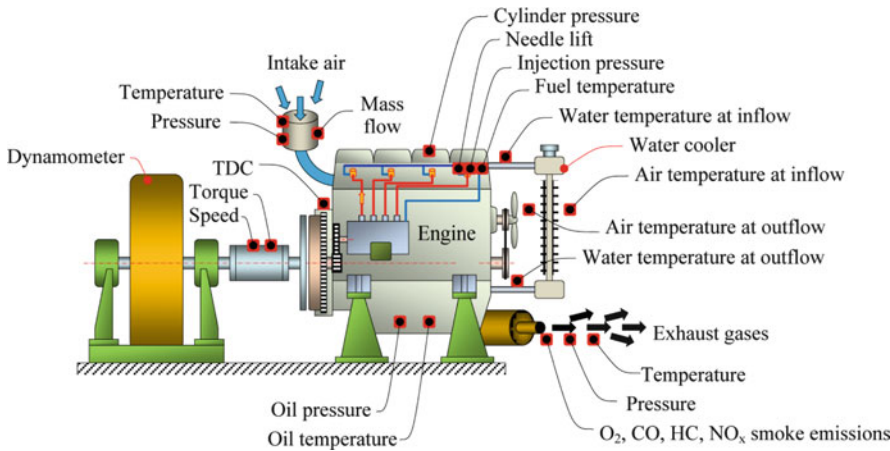


Fig. 2.30 Engine test bed scheme

Table 2.1 Techniques of emissions analysis

Gas	Technique
CO	Non-dispersive infrared (NDIR)
CO ₂	Non-dispersive infrared (NDIR)
NO _x	Chemiluminescence
Unburned hydrocarbons, HC	Flame ionization detector (FID), Fast FID
Hydrocarbon species, CH ₄	Fourier transform infrared (FTIR)
Particulate matter	Gravimetric analysis
Smoke	Filter method

The critical components for tribological assessment are presented schematically in Fig. 2.31.

To determine the alterations on *pump plunger surfaces* due to usage of various fuels, an *electron microscope* can be used. The surfaces have to be examined before and after fuel usage. To determine the influence of fuel usage on the *roughness* of the *pump plunger active surface*, the relevant roughness parameters have to be examined. The arithmetic roughness average R_a , the quadratic roughness average R_q , the maximum peak to valley height R_y , and the average peak to valley height R_z can be calculated on the basis of mechanical scanning of the pump plunger skirt surface and its head by a suitable device, for example, by the rotating head device PURV 3–100. It should be noted that a desired sliding surface (Fig. 2.32) exhibits a quasi-planar plateau separated by randomly spaced narrow grooves.

Carbon deposits on the injector and in the combustion chamber can be examined by *endoscopic inspection*. For this purpose an adequate videoscope system such as the OLYMPUS of type IPLEX SA with optical adapter IV76-AT120D/NF can be used.

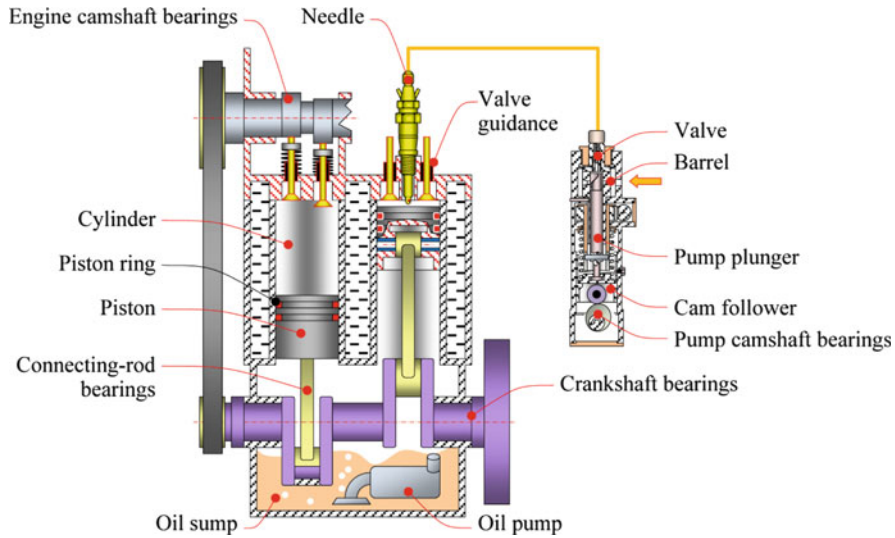


Fig. 2.31 Scheme of diesel engine with critical components for tribological assessment

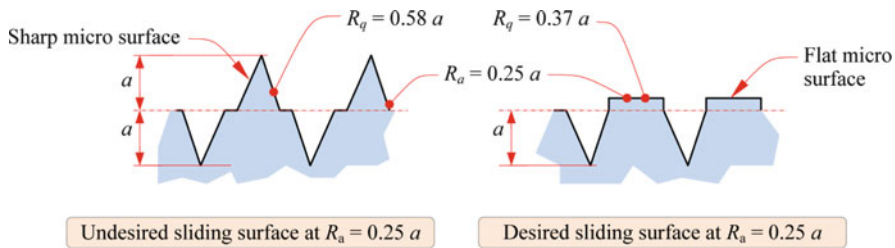


Fig. 2.32 Undesired and the desired sliding surfaces with equal roughness R_a

The *fuel flow coefficient* measuring device is intended to measure the fuel flow coefficients at steady-state conditions. The commonly used procedure is known as the Bosch procedure for measuring flow coefficients. The hydraulic scheme of the testing device is presented in Fig. 2.33.

The testing device consists of the calibrating fuel (CF) tank, filters, low pressure pump and high pressure pump (each pump is driven by its own electric motor), pressure chamber (to damp the pressure waves), restrictor, pressure regulating valve, directing valve (to direct the fuel flow into the desired measuring container), and nozzle holder for proper positioning of the testing nozzle. The needle position in the nozzle is calibrated by using a micrometer. Two pressure transducers for measuring the pressures before and after the high pressure pump are used. During the measurement, the temperature of the CF is regulated by a heat exchanger that is mounted into the fuel tank. For the calculation of fuel density, the fuel temperature in the measuring container is obtained by a thermoelement.

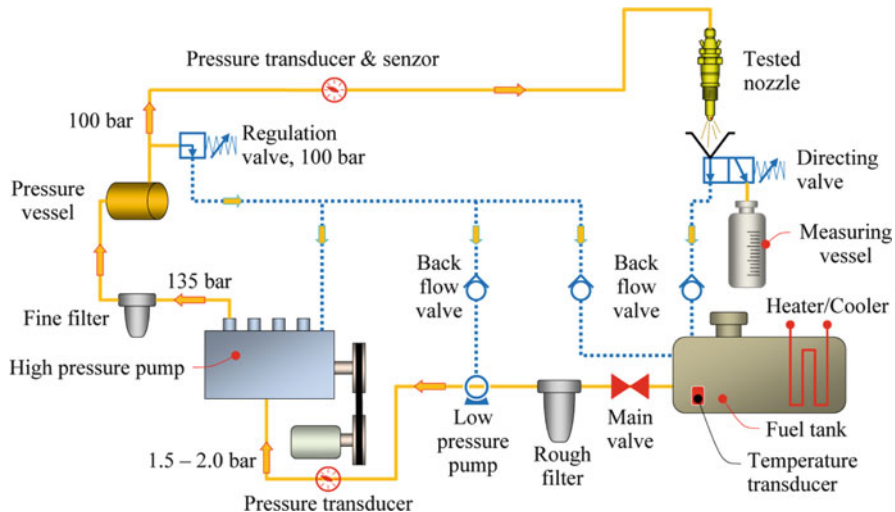


Fig. 2.33 Hydraulic scheme of the discharge coefficient testing device

The CF flows from the CF tank through the main valve and filter to the low pressure pump and further into the high pressure pump, through the high pressure tube and a micro-filter to the pressure chamber. This chamber acts like a damper for pressure oscillations. The pressure chamber is connected with the tested injector nozzle by the tube, equipped by the restrictor and a regulating valve. The restrictor is designed to regulate the flow of the fluid. The regulating valve is designed to keep the fluid pressure at constant value of 100 bar. The overflow of the injector goes through the nozzle leakage tube. Below the tested injector the directing valve is placed. This valve directs the fluid into the measuring container. The electromagnet of the directing valve is charged by the time switch, which can be precisely adjusted for the required duration of measurement. From the measured fuel quantity, the discharge coefficient can be calculated.

At the beginning of the measuring procedure, the required needle lift is set up by using a micrometer (Pehan et al. 2009). The fluid flows into the measuring container for some specified time interval (e.g., 30 s, 60 s, . . .) and at some specified pressure difference (e.g., 99 bar). By using the restrictor and the regulation valve, the pressure difference Δp is set to the required value. By using the time switch, the timer is started and the directing valve is activated, directing the fluid into the measuring container. After the prescribed time interval, the fluid flows through the injector back to the CF tank. On the basis of the fluid quantity in the measuring container and the time of measurement, the actual and the theoretical volume flows are calculated. The nozzle discharge coefficient μ is defined as the ratio between the measured (actual) volume flow \dot{V}_m and theoretical volume flow \dot{V}_t , injected through the nozzle, i.e., $\mu = \frac{\dot{V}_m}{\dot{V}_t}$. According to the Bernoulli equation, the theoretical outflow velocity through one nozzle hole can be derived from

the nozzle hole diameter d_{nh} , the pressure difference Δp , and fuel density ρ_f as $\dot{V}_t = \frac{\pi \times d_{nh}^2}{4} \sqrt{\frac{2 \times \Delta p}{\rho_f}}$. In general, the nozzle discharge coefficient has an important influence on the fuel spray characteristics and on injection characteristics (Kegl 2006).

2.3.2 Mathematical Modeling and Simulation

Computational fluid dynamics (CFD) modeling is becoming an attractive alternative for engine analysis in place of full experimental test stand study in recent years. It is broadly used by engine researchers to explore in-cylinder flow fields, heat transfer, combustion characteristics, and emission formation processes (Ismail et al. 2011; Gunabalan et al. 2010). The modeling of an internal combustion engine represents one of the most challenging fluid mechanics problems due to the compressible nature of the flow with large density variations, low Mach number, and turbulent, unsteady, cyclic, nonstationary, and nonuniform flow (Ismail et al. 2011). For the simulation of in-cylinder turbulent flow, a widely used Reynolds-averaged Navier–Stokes approach with RNG k – ϵ turbulence model is utilized as it accounts for high swirling flows (e.g., AVL FIRE and KIVA software).

In diesel engines, the combustion process can be categorized into two main phases, namely, the *premixed combustion* and *mixing-controlled combustion*. Premixed combustion is a rapid combustion process which heavily depends on the rate of atomization, breakup, vaporization, and mixing of the fuel droplets as well as chemical reactions. On the other hand, mixing-controlled combustion depends on the rate of turbulent mixing of fuel and air to form combustible mixture. A *non-premixed model* with the probability density function approach is used to model diesel combustion process for turbulent diffusion flames with fast chemistry (Ismail et al. 2011; Gunabalan et al. 2010).

Accurate and efficient numerical analysis is a key factor for successful determination of combustion characteristics and their improvements. For the steady-state performance prediction of diesel engines, there are several commercial packages (e.g., AVL BOOST) that are widely accepted, rigorously tested, and verified in practical applications.

The underlying mathematical models are based on the first law of thermodynamics. Basically, for the high pressure cycle this law states that the change of the internal energy in the cylinder $\left(\frac{d(m_c \times u)}{d\alpha}\right)$ is equal to the sum of piston work $(-p_c \times \frac{dV}{d\alpha})$, the conversion of chemical energy to the thermal energy $\left(\frac{dQ_f}{d\alpha}\right)$, heat transfer $\left(-\sum \frac{dQ_w}{d\alpha}\right)$, and the enthalpy flow due to blow-by $(-h_{BB} \times \frac{dm_{BB}}{d\alpha})$. For an internal combustion piston engine, it can be written as (Kegl 2011):

$$\frac{d(m_c \times u)}{d\alpha} = -p_c \times \frac{dV}{d\alpha} + \frac{dQ_f}{d\alpha} - \sum \frac{dQ_w}{d\alpha} - h_{BB} \times \frac{dm_{BB}}{d\alpha}, \quad (2.55)$$

where the symbol α denotes the angle of the crankshaft rotation, m_c is the mass of the mixture in the cylinder, u is the specific internal energy, p_c is the in-cylinder pressure, V is the cylinder volume, Q_f is the fuel energy, Q_w the heat transfer through the liner, and h_{BB} and m_{BB} are the enthalpy and mass of the mixture that escapes through the gap between the piston and the liner, respectively.

With the in-cylinder gas pressure p_c and the working displacement V_D of one piston, the indicated mean effective pressure p_i can be determined over the whole cycle duration as follows: $p_i = \frac{1}{V_D} \int_{CD} p_c dV$. Together with the gas equation:

$$p_c = \left(\frac{1}{V}\right) m_c R_o T_c, \quad (2.56)$$

where T_c is the in-cylinder gas temperature, equation (2.55) can be solved by using, for example, the Runge–Kutta method. Once the in-cylinder gas temperature is known, the in-cylinder gas pressure can be obtained from the gas equation.

To approximate the heat release characteristics of an engine, the Vibe function can be used:

$$x = 1 - e^{-ay(m+1)} \quad (2.57)$$

where x is the fraction of the fuel mass, which was burned since the start of combustion, $y = (\alpha - \alpha_o)/\Delta\alpha_c$, a is the Vibe parameter (a is usually equals 6.9 for complete combustion), m is the shape parameter (m usually equals 0.85), α is the angle of the crankshaft rotation, α_o is the angle of the combustion start, and $\Delta\alpha_c$ is the angle of combustion duration.

The actual heat release can be determined as

$$\frac{dQ_f}{d\alpha} = Q_{in} \left(\frac{dx}{d\alpha} \right), \quad (2.58)$$

where Q_{in} is the total heat input.

Furthermore, for the modeling of the heat transfer in the cylinder, the heat transfer coefficient α_w can be determined by using the heat transfer model Woschni, given by

$$\alpha_w = 130D^{-0.2} p_c^{0.8} T_c^{-0.53} \left(C_1 c_m + C_2 \left((V_D \times T_{c,1}) / (p_{c,1} \times V_{c,1}) (p_c - p_{c,o}) \right) \right)^{0.8}, \quad (2.59)$$

where D is the cylinder bore, c_m is the mean piston velocity, $p_{c,o}$ is the pressure of pure compression, $p_{c,1}$ and $T_{c,1}$ are the in-cylinder pressure and temperature (at the moment when the intake valve closes), and C_1 and C_2 are given constants.

The coefficient α_p of the heat transfer through the intake, $\alpha_{p,i}$, and exhaust, $\alpha_{p,e}$, ports can be described by the Zapf formulas for the intake and exhaust side, respectively, as

$$\begin{aligned}\alpha_{p,i} &= (C_7 + C_8 T_u - C_9 T_u^2) \times T_u^{0.33} \times \dot{m}^{0.68} \times d_{vi}^{-1.68} (1 - 0.765(h_v/d_{vi})), \\ \alpha_{p,e} &= (C_4 + C_5 T_u - C_6 T_u^2) \times T_u^{0.44} \times \dot{m}^{0.5} \times d_{vi}^{-1.5} (1 - 0.797(h_v/d_{vi})),\end{aligned}\quad (2.60)$$

where C_4 , C_5 , C_6 , C_7 , C_8 , and C_9 are given constants, \dot{m} is the mass flow, T_u is the temperature on the port input side, and d_{vi} and h_v are the valve seat diameter and the valve lift, respectively.

2.4 Discussion

Injection and fuel spray characteristics relate strongly to *engine performance, ecology, economy, and tribology characteristics*. All the most important injection characteristics like injection pressure, injection timing, injection duration, injection rate, and fuelling history, as well as fuel spray characteristics like spray tip penetration, spray angle, and Sauter mean diameter, determine mixture formation, in-cylinder pressure and temperature, self-ignition, and heat release. The engine combustion process is further strongly related to the engine power, torque, emissions, specific fuel consumption, carbon deposits, wear of engine parts, and so on. Unfortunately, the possibilities to control the combustion process directly are quite limited. In a mechanically controlled fuel injection system, even the injection process cannot be controlled directly. However, we can control injection indirectly through the fuel delivery process. For this reason, it is very important to know as good as possible the relationships among all injection, spray, and engine characteristics. Some of these relations are valid to a great extent for indirect and direct injection systems.

In general, low *injection pressure* enlarges the fuel droplet diameters and increases the *ignition delay* period during the combustion. This situation leads to an increase of the *in-cylinder pressure*, NO_x , and *CO emissions*. An increase of injection pressure typically improves the atomization at the nozzle outlet, resulting in a more distributed vapor phase, hence resulting in better mixing (Bruneaux 2001). When injection pressure is increased, fuel droplet diameters will become smaller and the mixing of the fuel with air during the ignition period improves, which leads to lower *smoke* level and *CO emission*. However, if the injection pressure is too high, the ignition delay becomes shorter. This worsens the mixing process and the combustion efficiency decreases. Consequently, smoke levels may rise (Celikten 2003). It has to be pointed out that the objective should be to increase the *mean injection pressure* to some reasonable maximum level. The maximum injection pressure is decisive for the mechanical loading of the fuel injection

pump's components and drive. In a mechanically controlled fuel injection system, the injection pressure increases together with increasing engine speed and load. During the injection process, the maximum injection pressure can be more than double of the mean pressure. Therefore, the maximum fuel injection pressure is also limited by the *strength* of engine materials, *wear* of various elements of the injection system, and engine system *cost*.

At higher mean injection pressure the *injection duration* becomes shorter, if the fuelling is kept constant. In order to keep specific fuel consumption, emissions of smoke, unburned HC, and NO_x at acceptable levels, the injection duration must be adjusted properly to the operating regime and the *start of injection*. A long injection period, caused by low *injection rate*, makes poor *spray tip penetration*. Moreover, if the injection period is too long, it would inevitably produce excessive *smoke* and *particulate* emissions. In this case a pilot injection might be of some benefit (Hwang et al. 1999).

The *injection timing* has a considerable influence on the *start of combustion* of the air–fuel mixture. In general, if the injection timing is advanced, the *in-cylinder temperature* increases, thus leading to an increase of NO_x emissions. The retarded injection timing leads to incomplete combustion and to higher unburned HC emissions (Jayashankara and Ganesan 2010).

Many studies confirm that the *injection rate history* affects *ignition* and *combustion* characteristics and the temporal history of *smoke* and NO_x formation in direct injection diesel engines (Juneja et al. 2004; Desantes et al. 1999; Hwang et al. 1999). Fuel injection quantity should be controlled by engine parameters such as engine speed, load, and air motion in the combustion chamber. In general, the fuel amount at the beginning of injection should be relatively small. After that it should be increased as the piston reaches the TDC and decreased after TDC to prevent too rapid increase of the combustion pressure. Therefore, injection rate modulation devices are being developed mainly to reduce this high initial heat release rate. A modulation device limits the fuel injected during the ignition delay period by a separated pilot injection, prior to the main injection, or by initial injection rate control. If the initial rate of injection is much lower during the main injection, less fuel is injected and mixed by the time the first element of fuel has evaporated to form a suitable mixture and autoignition occurs. Hence the initial heat release rate is low and consequently the combustion noise level is reduced. The main injection follows with most of the fuel injected. Ideally, the degree of separation between the initial and main injections should be longer when the ignition delay is long, for example, when engine is running at low load and low-speed conditions or under transient loads in urban traffic.

In order to improve the efficiency of diesel/biodiesel engine development, the injection, fuel spray, and engine characteristics unavoidably have to be investigated experimentally and numerically. The more or less sophisticated mathematical models addressed briefly in this section have been tested at many operating regimes and with various fuels. On the basis on the *comparison* of the *numerically* and *experimentally obtained results* one can say that these mathematical models may perform quite well. To illustrate this, some results are presented in the following.

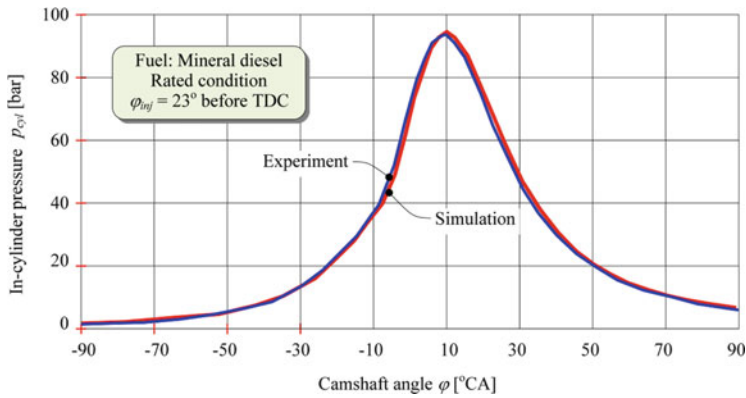


Fig. 2.34 Comparison of experimental and simulated in-cylinder pressure—AVL Boost

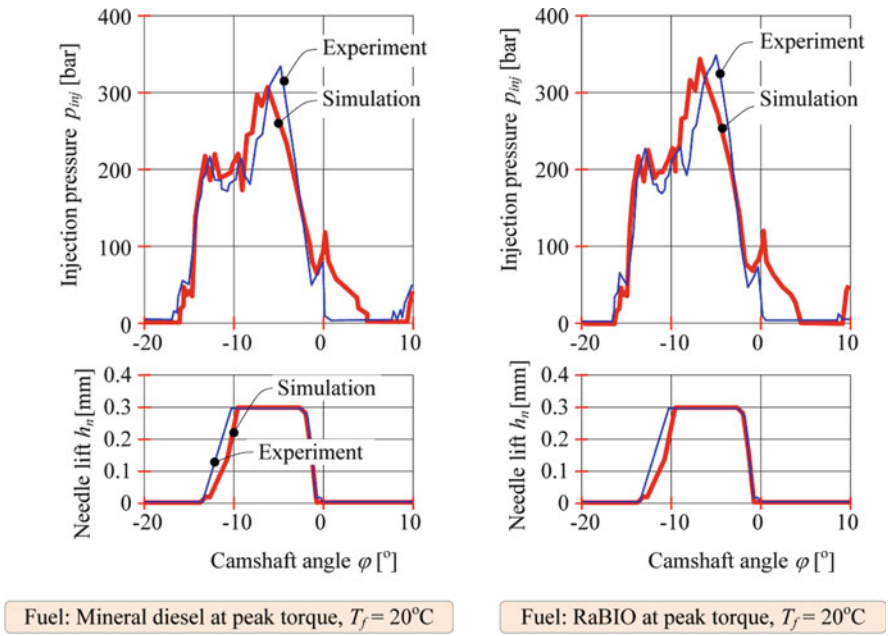


Fig. 2.35 Comparison of experimental and simulated injection characteristics—BKIN

A comparison of the in-cylinder pressure history of a diesel engine at rated conditions is shown in Fig. 2.34 (AVL Boost software).

The performance of the BKIN software is illustrated in Fig. 2.35. The given histories are for the diesel fuel M injection system of a MAN bus engine at peak torque condition. The used fuels are mineral diesel and rapeseed biodiesel.

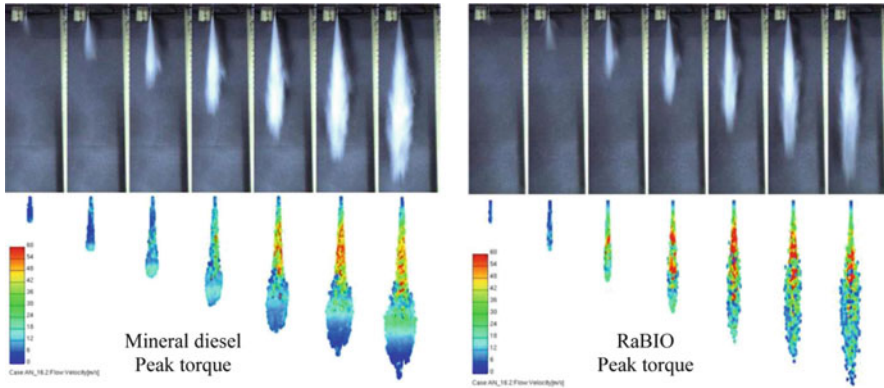


Fig. 2.36 Comparison of experimental and simulated fuel spray development—AVL FIRE

The performance of the mathematical model for fuel spray development (AVL FIRE software) at peak torque condition is illustrated in Fig. 2.36. Mineral diesel and rapeseed biodiesel fuels were analyzed.

At the end, it should be noted that commercially available software (e.g., Fire, Boost, Kiva, etc.) typically exposes a lot of user-definable coefficients of the models. Unfortunately, it is often not very easy to get/set proper values of these coefficients. Therefore great care should be put into proper determination of these coefficients in order to get reliable results and good agreement between experiment and simulation.

References

- Aigal, A. K. (2003). Analysis of measured droplet size distribution of air deflected diesel spray. *Proceedings of the Institution of Mechanical Engineers, Part D: Journal of Automobile Engineering*, 209, 33–43.
- Andreassi, L., Ubertini, S., & Allocca, L. (2007). Experimental and numerical analysis of high pressure diesel spray–wall interaction. *International Journal of Multiphase Flow*, 33, 742–765.
- Battistoni, M., & Grimaldi, C. N. (2012). Numerical analysis of injector flow and spray characteristics from diesel injectors using fossil and biodiesel fuels. *Applied Energy*, 97, 656–666.
- Bauer, H. (1999). *Diesel-engine management*. Stuttgart: SAE.
- Bruneaux, G. (2001). Liquid and vapour spray structure in high-pressure common rail diesel injection. *Atomization and Sprays*, 11, 533–556.
- Celikten, I. (2003). An experimental investigation of the effect of the injection pressure on engine performance and exhaust emission in indirect injection diesel engines. *Applied Thermal Engineering*, 23, 2051–2060.
- Desantes, J. M., Arrègle, J., López, J. J., & García, J. M. (2006). Turbulent gas jets and diesel-like sprays in a crossflow: A study on axis deflection and air entrainment. *Fuel*, 85(14–15), 2120–2132.

- Desantes JM, Arregle J, Rodriguez PJ (1999) Computational model for simulation of diesel injection systems, *SAE Paper* 1999-01-0915
- Desantes, J. M., Benajes, J., Molina, S., & Gonzalez, C. A. (2004). The modification of the fuel injection rate in heavy-duty diesel engines. Part 1: Effects on engine performance and emissions. *Applied Thermal Engineering*, 24, 2701–2714.
- Dukowicz, J.K. (1979). *Quasi-steady droplet phase change in the presence of convection*, Los Alamos Report LA-7997-MS
- Dukowicz, J. K. (1980). A particle-fluid numerical model for liquid sprays. *Journal of Computational Physics*, 35, 229–253.
- Gao, J., Matsumoto, Y., & Nishida, K. (2009a). Experimental study on spray and mixture properties of the group-hole nozzle for direct-injection diesel engines, part I: a comparative analysis with the single-hole nozzle. *Atomization and Sprays*, 19, 321–37.
- Gao, J., Matsumoto, Y., & Nishida, K. (2009b). Experimental study on spray and mixture properties of the group-hole nozzle for direct-injection diesel engines, part II: effects of included angle and interval between orifices. *Atomization and Sprays*, 19, 339–55.
- Gidaspow, D. (1994). *Multiphase flow and fluidization continuum and kinetic theory descriptions*. Boston, MA: Academic.
- Gosman, A. D., & Ioannides, E. (1983). Aspects of computer simulation of liquid-fueled combustors. *Journal of Energy*, 7, 482–490.
- Gunabalan, A., Tamilporai, P., & Ramaprabhu, R. (2010). Effect of injection timing and EGR on DI diesel engine performance and emission using CFD. *Journal of Applied Sciences*, 10(22), 2823–2830.
- Herzog, P. (1989). The ideal rate of injection for swirl supported diesel engines. IMechE, Diesel Fuel Injection Systems Seminar, Birmingham
- Heywood, J. B. (1988). *Internal combustion engines fundamentals*. New York, NY: McGraw Hill.
- Hiroyasu H, Arai M (1990) Structures of fuel sprays in diesel engines. *SAE Paper* 900475
- Hwang, J.W., Kal, H.J., Kim, M.H., Parkm, J.K., Shenghua, L., Martychenko, A.A., Chae, J.O. (1999). Effect of fuel injection rate on pollutant emissions in DI diesel engine. *SAE Paper* 1999-01-0195
- Ishiwata, H., et al. (1994) Recent progress in rate shaping technology for diesel in line pumps. *SAE Paper* 940194
- Ismail, H. M., Hg, H. K., & Gan, S. (2011). Evaluation of non-premixed combustion and fuel spray models for in-cylinder diesel engine simulation. *Applied Energy*, 90(1), 271–279.
- Iyer, V. A., Abraham, J., & Magi, V. (2002). Exploring injected droplet size effects on steady liquid penetration in a diesel spray with a two-fluid model. *International Journal of Heat and Mass Transfer*, 45(3), 519–531.
- Jayashankara, B., & Ganesan, V. (2010). Effect of fuel injection timing and intake pressure on the performance of a DI diesel engine—A parametric study using CFD. *Energy Conversion and Management*, 51, 1835–1848.
- Juneja H, Ra Y, Reitz RD (2004) Optimization of injection rate shape using active control of fuel injection. *SAE Paper* 2004-01-0530
- Kegl, B. (1995). Optimal design of conventional in-line fuel injection equipment. *Proceedings of the Institution of Mechanical Engineers, Part D: Journal of Automobile Engineering*, 209, 135–141.
- Kegl, B. (1996). Successive optimal design procedure applied on conventional fuel injection equipment. *Journal of Mechanical Design*, 118(4), 490–493.
- Kegl, B. (1999). A procedure for upgrading an electronic control diesel fuel injection system by considering several engine operating regimes simultaneously. *Journal of Mechanical Design*, 121(1), 159–165.
- Kegl, B. (2004). Injection system optimization by considering fuel spray characteristics. *Journal of Mechanical Design*, 126, 703–710.
- Kegl, B. (2006). Experimental investigation of optimal timing of the diesel engine injection pump using biodiesel fuel. *Energy Fuels*, 20, 1460–1470.

- Kegl, B. (2008). Effects of biodiesel on emissions of a bus diesel engine. *Bioresource Technology*, 99, 863–873.
- Kegl, B. (2011). Influence of biodiesel on engine combustion and emission characteristics. *Applied Energy*, 88, 1803–1812.
- Kegl, B., & Hribernik, A. (2006). Experimental analysis of injection characteristics using biodiesel fuel. *Energy fuels*, 20(5), 2239–2248.
- Kegl, B., Kegl, M., & Pehan, S. (2008). Optimization of a fuel injection system for diesel and biodiesel usage. *Energy & Fuels*, 22, 1046–1054.
- Kegl, B., & Müller, E. (1997). Design of cam profile using Bézier's curve. *Journal of Mechanical Engineering*, 43(7–8), 281–288.
- Lee, C. S., & Park, S. W. (2002). An experimental and numerical study on fuel atomization characteristics of high-pressure diesel injection sprays. *Fuel*, 81, 2417–2423.
- Leng, X., Feng, L., Tian, J., Dua, B., Long, W., & Tian, H. (2010). A study of the mixture formation process for a third-generation conical spray applied in HCCI diesel combustion. *Fuel*, 89, 392–398.
- Liu AB, Reitz RD (1993) Modeling the effects of drop drag and breakup on fuel sprays, *SAE Paper* 930072
- Merker, G.P., Schwarz, C., Stiesch, G., Otto, F. (2005). *Simulating combustion*. Springer
- Moon, S., Matsumoto, Y., Nishida, K., & Gao, J. (2010). Gas entrainment characteristics of diesel spray injected by a group-hole nozzle. *Fuel*, 89, 3287–3299.
- Myong, K. J., Suzuki, H., Senda, J., & Fujimoto, H. (2008). Spray inner structure of evaporating multi-component fuel. *Fuel*, 87, 202–210.
- Naber JD, Reitz RD (1988) Modeling engine spray/wall impingement, *SAE Paper* 880107
- Needham J (1990) Injection timing and rate control—a solution for low emissions. *SAE Paper* 900854
- O'Rourke PJ (1980) Modeling of drop interaction in thick sprays and a comparison with experiments, IMechE—Stratified Charge Automotive Engines Conference
- Payri, R., García, J. M., Salvador, F. J., & Gimeno, J. (2005). Using spray momentum flux measurements to understand the influence of diesel nozzle geometry on spray characteristics. *Fuel*, 84, 551–561.
- Pehan, S., Svoljšak-Jerman, M., Kegl, M., & Kegl, B. (2009). Biodiesel influence on tribology characteristics of a diesel engine. *Fuel*, 88, 970–979.
- Plint, M., & Martyr, A. (1995). *Engine testing theory and practice*. Manchester: Butterworth-Heinemann.
- Pogorevc, P., Kegl, B., & Škerget, L. (2008). Diesel and biodiesel fuel spray simulations. *Energy & Fuels*, 22, 1266–1274.
- Rad, G. J., Gorjiinst, M., Keshavarz, M., Safari, H., & Jazayeri, S. A. (2010). An investigation on injection characteristics of direct injected heavy duty diesel engine by means of multi-zone spray modeling. *Oil and Gas Science and Technology—RevIFP Energies nouvelles*, 65(6), 893–901.
- Sazhina, E. M., Sazhin, S. S., Heikal, M. R., Babushok, V. I., & Johns, R. J. R. (2000). A detailed modelling of the spray ignition process in diesel engines. *Combustion Science and Technology*, 160(1–6), 317–344.
- Soid, S. N., & Zainal, Z. A. (2011). Spray and combustion characterization for internal combustion engines using optical measuring techniques—A review. *Energy*, 36, 724–741.
- Tatschl R, Künsberg Sarre C, Berg E (2002) IC-Engine spray modeling – status and outlook, International Multidimensional Engine Modeling User's Group Meeting at the SAE Congress 2002.
- Zhang, G., Qiao, X., Miao, X., Hong, J., & Zhen, J. (2012). Effects of highly dispersed spray nozzle on fuel injection characteristics and emissions of heavy-duty diesel engine. *Fuel*, 102, 666–673.

Green Diesel Engines

Biodiesel Usage in Diesel Engines

Kegl, B.; Kegl, M.; Pehan, S.

2013, VII, 263 p. 217 illus., Hardcover

ISBN: 978-1-4471-5324-5